Rheological and mechanical behavior of soy protein-polysaccharide composite paste for extrusion-based 3D food printing: Effects of type and concentration of polysaccharides

Jian Wang, Quanjin Jiang, Zhenyu Huang, Ahsan Hafiz Muhammad, Adem Gharsallaoui, Ming Cai, Kai Yang, Peilong Sun

Rheological and mechanical behavior of soy protein-polysaccharide composite paste for extrusion-based 3D food printing: effects of type and concentration of polysaccharides

Jian Wang [a b †], Quanjin Jiang [a †], Zhenyu Huang [a], Ahsan Hafiz Muhammad [a], Adem Gharsallaoui [c], Ming Cai [a b *], Kai Yang [a b *], Peilong Sun [a b *]

[a] College of Food Science and Engineering, Zhejiang University of Technology, Chaowang 18, Hangzhou 310014, Zhejiang, China

[b] Key Laboratory of Food Macromolecular Resources Processing Technology Research (Zhejiang University of Technology), China National Light Industry, Hangzhou 310014, Zhejiang, China

[c] CNRS, LAGEPP UMR 5007, Univ. Lyon, University Claude Bernard Lyon 1, 43 Bd 11 Novembre 1918, Villeurbanne, 69622, Lyon, France

[*] Corresponding authors: caiming@zjut.edu.cn (M.C.); yangkai@zjut.edu.cn (K.Y.); sun_pl@zjut.edu.cn (P.S.); Tel.: +86-0571-88813775; Fax.: +86-0571-88813778.

[†] These authors contributed equally to this work.

Abstract

Soy protein isolate (SPI)-based pastes are widely employed for 3D printing of food materials. However, their rheological properties often do not meet the 3D printing requirements. To enhance the 3D printing characteristics of SPI pastes, this study combined SPI with carrageenan and sodium alginate to form composite materials. The effect of polysaccharide type and concentration on the rheological and textural properties of the ink was investigated to elucidate the mechanism of interaction between proteins and polysaccharides. The results demonstrated that the addition of carrageenan (1.5%, wt %) and sodium alginate (1.5%, wt %) effectively improved the mechanical properties of the paste, such as hardness and adhesiveness, enhanced thus the quality of 3D printed products. With the increase of polysaccharide proportion, the apparent viscosity and storage modulus (G') of the composite paste increased significantly. Fourier-transform infrared spectroscopy (FT-IR), protein solubility measurement, X-ray diffraction (XRD), and differential scanning calorimetry (DSC) were employed and the results revealed notable interactions among SPI and two kinds of polysaccharides, with electrostatic interactions and hydrophobic interactions being the primary driving forces. The addition of polysaccharides induced changes in the paste crystalline state and improved its thermal stability. Scanning electron microscopy (SEM) confirmed a uniform and compact microstructure due to the incorporation of polysaccharides. Consequently, the SPI-polysaccharide paste can be considered as novel material for 3D printing food materials, and the results of this study provides a theoretical foundation for its application in the field of plant-based food products.

Keywords: 3D printing; SPI-polysaccharide composite paste; Printability; Rheological properties

1. Introduction

3D printing is an efficient and convenient processing technology. Because of its bottom-up stacking approach, can print and manufacture complex and complicated structures that traditional processing methods cannot construct (Dankar et al., 2018). It has broad applications in various fields such as textiles, architecture, healthcare, and food (Keerthana et al., 2020). 3D food printing is revolutionizing the food processing industry by creating novel foods with complex shapes, distinctive textures, and enhanced nutritional value. This allows for personalized nutrition and customized food design, catering to the specific needs of aging populations, children, and sick patients. (Phuhongsung et al., 2020). Typically, extrusion, binder jetting, and inkjet printing technologies have been explored for various 3D food printing applications (Cheng et al., 2022). Among them, extrusion-based printing technique can be effectively used for semi-solid pastes such as grain dough, meat puree, and chocolate. The principle of this technique is to extrude material layer by layer through a nozzle to form a complex 3D structure (Rowat et al., 2021). Extrusion technology is currently the most widely studied method for 3D food printing. The emergence of 3D food printing technology helps to accelerate the development of new food products and become a potential technological mean to rebuild the conventional food supply chain (Chen et al., 2019).

Proteins and polysaccharides are two essential nutrients in the human food system that can alter their structural and functional properties, such as the ability to form gels or emulsions, through electrostatic forces and hydrogen bonds (Zhang et al., 2022). Soy protein isolate (SPI) as a food component has been widely used in 3D printing (Chen et al., 2019; Phuhongsung et al., 2020). However, SPI exhibits limitations in terms of printing accuracy and stability, as it is prone to breakage under high shearing forces. To address this issue, the addition of hydrocolloids or salt ions to SPI has been identified as a viable solution (Xu et al., 2023). Previous research has demonstrated the effectiveness of incorporating apricot polysaccharide into SPI, resulting in improved gelatinization performance and viscoelasticity of the SPI gel (Xu et al., 2023). Polysaccharide is a kind of natural macromolecular carbohydrate with complex and huge molecular structure obtained from multiple monosaccharides after dehydration

and condensation. Although polysaccharides are widely distributed in nature, not all polysaccharides are called food polysaccharides. Food polysaccharide refers to the polysaccharide that is allowed as a food additive in the food processing process to control the sensory quality, physical properties and improve the nutritional value of food. Kappa-Carrageenan (κC), a widely used polysaccharide in the food industry, exhibits rapid thermal-reversible behavior and can form robust and brittle gel structures suitable for 3D printing (Liu et al., 2019; Yu et al., 2022). Additionally, alginates are widely used as 3D printing materials because of their good gelling properties due to their many carboxyl and hydroxyl groups (Chen et al., 2019). Dick et al. (2020) investigated the effects of different ink polysaccharides on the rheology and texture of pig meat and found that the addition of ink polysaccharides improved the printability and texture of the meat. Studies have reported that SPI mixed with sodium alginate and gelatin as a 3D printing material improved the hardness and chewiness of 3D printed geometries, and SPI paste will be a promising material for 3D food printing (Chen et al., 2019).

Currently, 3D printing of food is still in its early stages. Warner et al. (2019) investigated the 3D printability of a mixture of gelatin and κC and found that the addition of κC resulted in a more stable structure than pure gelatin. Commercially, the 3D printed plant-based beef product “Alt Steak” produced by Israeli startup Redefine Meat has been sold in over 120 restaurants in Israel, the Netherlands, Germany, and the United Kingdom. Japanese company “Open Meals” uses 3D printer to print edible pixelated sushi. Each sushi is composed of edible gel with specific color and taste. However, to date, there has been limited exploration of 3D printing of SPI-polysaccharide composite pastes. At the same time, carrageenan and sodium alginate are extracted from plants, and we consider maintaining a plant-based property in the material properties of the ink, which can be used as a raw material to support the production of plant meat in the future. Therefore, this study developed a 3D printable ink by mixing SPI with κC and alginate polysaccharides. The structural and functional properties of the ink were evaluated using rheology, texture analysis, Fourier transform infrared spectroscopy, and scanning electron microscopy. The study investigated the

interactions between protein and polysaccharides and their effects on the printability of the ink.

2. Materials and methods

2.1. Materials

SPI (protein content > 90%) was purchased from Shanghai yuanye Bio-Technology Co., Ltd (Shanghai, China). The ionic content of SPI was determined by atomic absorption spectrometry, and its composition was 0.02±0.01 wt% of Ca^{2+}, 0.04±0.00 wt% of K^{+} and 0.03±0.01 wt% of Na^{+}. Kappa-carrageenan (κC) and β-mercaptoethanol were acquired from Shanghai Aladdin Ltd (Shanghai, China). The ionic content of κC was determined by the same procedure, the contents were 3.5±0.05 wt% of K^{+}, 1.25±0.01 wt% of Na^{+}, 0.47±0.04 wt% of Ca^{2+}, 2.1±0.02 wt% of Cu^{2+}, and 3.2±0.03 wt% of Zn^{2+}. Sodium alginate (SA), tris (hydroxymethyl)methyl aminomethane (Tris), glycine, urea, sodium dodecyl sulfate (SDS), and disodium ethylenediaminetetraacetic acid (Na_2EDTA) were supplied by Shanghai Macklin Biochemical Technology Co., Ltd (Shanghai, China). The ionic content of SA was determined by the same procedure, the contents were 2.31±0.01 wt% of K^{+}, 11.23±0.02 wt% of Na^{+}, 0.03±0.01 wt% of Fe^{2+}. Bovine serum albumin (BSA) was obtained from Solarbio Science & Technology Co., Ltd (Beijing, China). All other reagents and chemicals were of analytical grade.

2.2. Food 3D Printing Ink Preparation

The mixtures of SPI with sodium alginate and κC were prepared as followed. SA and κC solutions were dissolved in deionized water at three concentrations (1, 1.5, and 2% w/w). Subsequently, mixed the two solutions and added SPI powder to the mixed solution to achieve a concentration of 15% (w/w) of SPI. Table 1 presents eight representative ink formulations with a gradient cross rise in two kinds of polysaccharides, the original ratio of SPI and polysaccharide was chosen according to Hu et al., (2017). The resulting mixed solution was homogenized using a homogenizer (HFJ-25, Hengao, Tianjin, China) at 500 rpm for 5 min until a stable suspension was formed. All samples had pH values within 6.8±0.3, which were above the isoelectric point of soy proteins (Lu et al., 2023). The resulting paste-like mixture was kept in a

water bath at 80 °C for 30 min and cooled at room temperature for 15 min. The samples were stored overnight in the refrigerator and heated to 25 °C before 3D printing.

2.3. 3D printing process

The samples were printed using an extrusion-based food 3D printer (FOODBOT-S2, Hangzhou Shiyin Technology Co., Ltd., Hangzhou, China). The prepared ink filled into the 3D printing nozzle syringe, and the printer extruded the material by controlling the movement of the plunger in accordance with the preset 3D mesh model (18.6 mm × 18.6 mm × 8 mm). The main printing parameters were set as follows: nozzle diameter of 0.84 mm, nozzle printing rate of 25 mm/s, layer height of 0.8 mm, printing temperature of 25 °C, extruded rate of 24 mm^3/s and infill density of 100% printing. To ensure maximum aseptic operation, all containers, nozzle syringes, and nozzle tips were sterilized at 121 °C in an autoclave for 15 min. The printing environment was disinfected with 75% ethanol and UV radiation, and all operations were conducted in a laminar flow hood.

2.4. Rheological Properties of Printing Inks

The rheological properties of the printing inks were measured using a hybrid rheometer (Discovery HR-2, DHR, TA Instruments, New Castle, DE, USA). A parallel plate with a diameter of 40 mm was used, with a measurement gap of 1 mm. When loading the sample, any excess material on the edges was removed with a scraper, and a thin layer of silicone oil was applied to the edges to prevent moisture evaporation. The configuration was set as follow: soak time was 180 s, 7 points were detected per decade, the interval between the points was 10 s, and the steady state sensing in DHR rheometer was applied to make sure the equilibrium time was 30 s for each point.

2.4.1. Flow sweep test

The flow sweep test was measured at shear rates ranging from 0.01 to 100 s^{-1}, with a temperature set at 25 °C, to obtain the viscosity η as a function of shear rate and investigate the shear-thinning behavior of the sample.

2.4.2. Amplitude sweep test

The linear viscoelastic region (LVR) was determined through an amplitude sweep test. The test was conducted within a strain range of 0.01-100% at a constant frequency

of 10 rad/s, and the experiment was performed at a temperature of 25 °C.

2.4.3. Frequency sweep test

The dynamic viscoelastic properties of the sample were evaluated through a frequency sweep test. The oscillation was performed within a frequency range of 0.1-100 rad/s, with a constant strain of 0.5% (within the LVR), and the experiment was conducted at a temperature of 25 °C. The storage modulus (G') loss modulus (G") and loss tangent (tan $\delta = G''/G'$) were recorded. All tests were repeated in triplicates, and experimental curves were plotted accordingly.

2.5. Texture analysis

Texture characteristics of the 3D printed samples were measured using a texture analyzer (TA. XT Plus, Stable Micro Systems, UK) equipped with a P36/R probe. The samples were tested as 18.6 × 18.6 × 8 mm grid-like architectures printed products for two compression cycles. The testing parameters were set as follows: the pre-test, test, and post-test speeds were all set at 1 mm/s, the trigger force was 10 g, the compression ratio was 50%, the time interval between the two compressions was 5 s, and the measurement temperature was 25 °C. Each sample was tested three times for repeatability.

2.6. Field-emission Scanning electron microscopy (FE-SEM) analysis

The microstructure of the paste was observed using a scanning electron microscope. The paste samples were freeze-dried, and the surface of the samples was sputter-coated with gold under vacuum conditions. The samples were then observed under the field-emission scanning electron microscope (S-4700, HITACHI, Japan) at different magnifications (1000×, 2500× and 5000×) with an accelerating voltage of 15 kV.

2.7. Molecular interaction analysis

To elucidate the paste cross-linking mechanism resulting from SPI-polysaccharide interactions, the protein solubility of the composite paste in five different solvents was measured to assess the intermolecular forces within the paste according to the method described by Wang et al. (2018). The paste sample (protein concentration 2 mg/mL) was dissolved in different solvents. The solvent S1 was distilled water, the solvent S2 consisted of 0.086 M Tris-0.09 M Glycine-4 mM-Na_2EDTA (pH = 8.0), the solvent S3

was 0.5% SDS, the solvent S4 was 8 M Urea, and solvent S5 was 2% β-mercaptoethanol. The mixture samples (2.00 ± 0.02 g) were mixed with 10 mL buffer, the resulting solution was incubated in a water bath at 25 °C for 20 min, and then centrifuged at 5000 rpm for 10 min. The protein supernatant was determined using bovine serum albumin as standard with ultraviolet spectrophotometry at 595 nm (GENESYS 150, Thermo Fisher Scientific Inc, Waltham, MA, USA). The protein solubility is expressed as the percentage of protein content of the supernatant in the total protein content.

Tris-glycine buffer disrupts electrostatic interactions, SDS disrupts hydrophobic interactions by disrupting the medium between the hydrophobic and hydrophilic regions, urea disrupts hydrogen bonding in the protein by dehydrating the protein molecules' side chains and backbone, and β-mercaptoethanol reduces protein disulfide bonds by competing with thiol groups (Qin et al., 2017; Wang et al., 2021). According to this method, the differences in protein solubility in S2 (Tris-Gly buffer)-S1 (distilled water), S3 (0.5% SDS)-S2, S4 (urea)-S3, and S5 (β-mercaptoethanol)-S4 were used as indications of the electrostatic interactions, hydrophobic interactions, hydrogen bonding interactions, and disulfide bonding interactions, respectively.

2.8. Fourier transform infrared spectroscopy (FTIR)

The samples were mixed with dry KBr at a ratio of 1:100 (w/w). Then the mixed powder was ground in the quartz mortar and pressed into a tablet. FTIR spectra (Nicolet 6700, Thermo Fisher Scientific Inc, USA) was performed at 25 °C in the range of 4000 to 500 cm^{-1}. The resolution remains at 1 cm^{-1}.

2.9. X-ray diffraction (XRD)

The X-ray diffraction (XRD) patterns of Cu Kα radiation (λ = 0.1541 nm) were recorded by powder diffractometer (Empyrean, Malvern PANalytical, NL). The working voltage was 40 kV and the working current was 40 mA. The patterns were collected with a 2θ range from 5° to 60° at a step of 0.0262°.

2.10. Differential scanning calorimetry (DSC)

Differential scanning calorimeter (DSC 8000, PE Instruments Inc., USA) was used to evaluate the thermal properties of the composite pastes. The thermal analysis was conducted according to the method described by Wang et al. (2018) with slight

modifications. Briefly, the sample mixture (10 mg) was accurately weighed and loaded into a DSC pan. Prior to analysis, the DSC pan was sealed and maintained at the initial scanning temperature of 20 °C. The sample was analyzed from 20 °C to 180 °C at a scanning rate of 10 °C/min, and the temperature of each endothermic or exothermic peak was determined. A sealed empty pan was used as a blank reference.

2.11. Statistical Analysis

The results are shown as the mean ± standard deviation (SD) of triplicate experiments. SPSS software (SPSS26; IBM SPSS Statistics, Chicago, IL, USA) was used for one-way ANOVA and Duncan tests at 95% confidence level for data analysis. All graphs in the experiment were drawn using Origin software (2020b, OriginLab, MA, USA).

3. Results and discussion

3.1. Printability of composite inks

Soy protein isolate (SPI), as the main material for printing, cannot be directly printed due to its high flowability and relatively weak cross-linking in water (Shi et al., 2023). Sodium alginate (SA) is a commonly used hydrophilic colloid with good binding capacity for proteins (Chen et al., 2022). Kappa-carrageenan (κC) is a soluble polysaccharide with high solubility and gelation properties (Bi et al., 2018). The addition of SA and κC to the SPI paste could improve the stability and printability of food ink. In order to screen ink formulations with optimal printing performance, this study prepared inks with different polysaccharide concentration ratios and examined their printability. The 3D printing results of different ink formulations are shown in Figure 1. The successful implementation of food 3D printing requires two conditions: the material in the extrusion process has the right viscosity to flow through the nozzle and adhere layer by layer, and the paste structure after extrusion has sufficient mechanical strength to ensure its formability (Osi et al., 2021). For preliminary tests of printability, the ink should be continuously extruded from the nozzle as a uniform filament, and the printed product should show the effect of perfect detail, smooth surface, and structural stability, rather than being unable to form or causing blockages and tangled (Figure 1).

In the blue irregular region, SPI paste collapsed immediately after continuous and uniform extrusion from the nozzle, showing the characteristics of some liquid-like fluids, and the 3D printing molding effect was poor, unable to form and support the designed three-dimensional grid structure. This could be due to the insufficient gelation capacity and the low viscosity, and the ink forms irregular printing filaments at the nozzle, resulting in the inability to form a homogeneous structure (Jiang et al., 2019). In the orange region, the ink formulation aggregates significantly at the nozzle when subjected to stress, which may be due to the inappropriate surface tension of the ink, leading to a tendency for rapid recovery and aggregation of the system after extrusion (Fu et al., 2021). In the gray region, as the polysaccharide content in the ink gradually increased, the viscosity of the sample increased, resulting in poor flowability of the ink material and the nozzle clogging (Fu et al., 2021). In the green printable region, ink components were able to be continuously and smoothly extruded. The ink can be printed when the concentration of SA changed from 1 wt% to 2.5 wt% with a κC concentration of 1 wt%, or when the concentration of SA changed from 1 wt% to 2.5 wt% with a κC concentration of 1.5 wt%. However, some ink formulations, such as S15A1K1.5, S15A1K1, and S15A1.5K1.5, print three-dimensional mesh structure filaments that are uneven and have broken structures. In contrast, the 3D mesh structures printed by the SPI15A1.5K1 and S15A2K1.5 formulations had good self-supporting properties, smooth surfaces and showed uniform layer thickness. Therefore, to investigate the reasons for the differences in printability among the different formulations and the effects of different polysaccharide concentrations on ink printability, five representative ink formulations (irregular: SPI 15; tangled: S15A2K2; clogged: S15A1.5K2; printable: S15A1.5K1.5 and S15A2K1.5) were selected for in-depth study.

3.2. Rheological properties

The rheological properties of the inks directly influence their printability for 3D printing based on extrusion samples, with viscosity being a key indicator of extrusion capability. As the polysaccharide concentration increased, the viscosity of the paste also increased. As shown in Figure 2a, all samples exhibited a shear rate-dependent

reduction in viscosity, demonstrating typical shear-thinning behavior, which is generally favorable for extrusion-based 3D printing (Dankar et al., 2018). This may be attributed to the disruption of polymer entanglement during the shear process, causing polymer chains to stretch and align parallel to the shear direction (Hou et al., 2022; Zhang et al., 2022). The stress and shear rate applied to the fluid during extrusion depends on the fluid and extrusion conditions, and these conditions can vary greatly in different applications (Lopez Hernandez et al., 2021). The apparent shear rate of a steady-state pipe can be derived by extruding the corresponding flow rate and tube radius (Xie et al., 2020).

$$\dot{\gamma} = \frac{3.34Q}{\pi R^3}$$

Where Q is the volumetric flow rate and R is the tube inner radius. According to the volumetric flow (24 mm^3/s) and inner radius (0.42 mm), the calculated shear rate is about 344.4 s^{-1}. This result is fitted with the report of (Lopez Hernandez et al., 2021). The viscosity of the SPI 15 ink at the high shear rate (100 s^{-1}) is much lower than the viscosity at the low shear rate of 0.1 s^{-1}. This is because at very low shear rates, the stable aggregates formed by the glycine subunits of SPI are stabilized by disulfide bonds, and the side chains are entangled with adjacent chains, resulting in high viscosity. As the shear rate increases, the unraveling of the side chains and the arrangement of the molecules provide less shear resistance, thereby reducing the viscosity (Dorishetty et al., 2019). Some studies have added *Lycium barbarum* polysaccharide to soy protein isolate, and the results show that the apparent viscosity increases significantly with the addition of polysaccharide in a concentration-dependent manner (Xing et al., 2024). In our experiment, the slope of the viscosity versus shear rate was not smooth, which is also observed in other studies (Lu et al., 2023, Liu et al., 2022, Yu et al.,2022 and Chen et al., 2019). This may be because the sample has not yet reached equilibrium, especially at a high shear rate. In the high shear rate region (i.e. from 1 to 100·s^{-1}), molecules or particles within the fluid may not have enough time to rearrange and adjust their positions. Besides, it is speculated that the turbulent flow happened or the sample slipped out at the higher shear rate. At the shear rate of 1 s^{-1}, the viscosity of S15A1.5K2,

S15A1.5K1.5, and SPI 15 food inks was 1.22×10^3 Pa s, 9.81×10^2 Pa s and 9.06×10^2 Pa s, respectively. The viscosity range of S15A1.5K1.5 ink is similar to the results of (Dick et al., 2020). Among them, the viscosity of more than 1200 Pa s will lead to entanglement of ink molecules, insufficient pressure in the cylinder, resulting in nozzle clogging. If the viscosity was less than 900 Pa s, although it is easy to squeeze, the fluidity was too large to provide sufficient viscoelasticity and stability. Therefore, an ideal viscosity for the ink should be known during the extrusion process, which allows the ink to pass through the narrow diameter of the printing nozzle while maintaining its deposition structure and shape.

The nonlinear rheological behavior of samples can be monitored by large amplitude oscillatory shear test. The linear viscoelastic range (LVER) and critical strain of ink formulations with different compositions are shown in Figure 2b. LVER is a range where the storage modulus G' and loss modulus G" remain relatively constant as shear intensity increases. The G' is a measure of the elastic solid-like behavior, that is, the resistance to elastic deformation of the sample, while the G" is the viscous response, which is the ratio of stress to strain under vibration conditions (Yang et al., 2018). When G' is greater than G", the material behaves primarily as a solid, and vice versa for a viscous fluid, exhibited a slight frequency dependence (Pan et al., 2022). Within this range, the material undergoes elastic deformation and can recover to its original state after the stress is removed. As shown in Figure 2b, when the applied strain is less than 1%, different inks have similar LVERs, maintaining stable values. As the strain increased, the value of G' started to decrease, indicating the critical point of the elastic properties of the samples about 1-2%. The weak gelation ability of SPI at room temperature results in disordered polymer chains and poor stability, leading to a liquid-like state after extrusion (Fu et al., 2021). There is a clear positive correlation between G' and the polysaccharide concentration in the ink, where G' increases sequentially for inks S15A1.5K1.5 and S15A2K1.5, indicating higher structural strength, which aligns with the results of viscosity tests. Among them, ink S15A1.5K1.5 showed the lowest G' value in all the ink formulations with added polysaccharides. This may be due to a low polysaccharide concentration, which prevents the ink system from forming a stable

paste structure.

Frequency sweep tests can provide information about the internal structure of the printing inks (Hou et al., 2022). As shown in Figure 2c and, 2d, the G' and G" of all pastes exhibit a steady upward trend, with G' being superior to G", indicating that the ink primarily possesses elastic and solid characteristics. Higher polysaccharide content in the paste could leads to higher cross-linking density in the SPI-polysaccharide system, resulting in stronger viscoelasticity and mechanical strength of the paste, as well as good self-supporting properties and resistance to shape deformation (Pan et al., 2022). This might be attributed to the formation of a denser and more robust intermolecular cross-linking structure through molecular interactions between polysaccharides and SPI, exhibiting stronger solid characteristics. The loss tangent, tan δ = G"/G', is used as a characteristic parameter to account for the different viscoelastic behaviors. A tan δ value less than 1 indicates a predominantly elastic property, while a tan δ value greater than 1 indicates a predominantly viscous property (Yang et al., 2018). The tan δ values of all samples were less than 1, which indicated that the addition of polysaccharide enhanced the gel properties of the mixture and made it form a rigid gel structure. The addition of κC can induce electrostatic interactions with proteins, leading to the predominant solid-like behavior of these fluids (Lu et al., 2022). Among them, with a constant κC concentration of 1.5 wt% and angular frequency of 10 rad/s, when the SA concentration was increased from 1.5 wt% to 2 wt%, G' and G" increase from 24970.3 Pa and 4042.66 Pa to 30697.3 Pa and 4845.1 Pa, respectively. G' increased by 22.94% and G" increased by 19.85%. However, with a constant SA concentration of 2 wt% and angular frequency of 10 rad/s, when the κC concentration was increased from 1.5 wt% to 2 wt%, G' and G" increased from 30697.3 Pa and 4845.1 Pa to 32279.5 Pa and 5002.04 Pa, respectively. G' increased by 51.54% and G" increased by 3.24%. These results suggest that polysaccharides participate in the formation of the paste structure, and different types of polysaccharides lead to different structures. It has been reported that with the increase of κC concentration, the interaction between κC-proteins may gradually decrease and be replaced by the κC-κC interaction (Lu et al., 2022). Some studies have shown that the gel strength of calcium alginate gels is relatively weak (Fernández Farrés

et al., 2013). Compared to SA, κC has a greater impact on the viscoelasticity of the paste, and at higher concentrations, the paste structure becomes more rigid. However, excessively high viscoelasticity of the paste may have adverse effects on 3D printing, as the generated high shear forces can hinder ink extrusion or cause fracture after extrusion. On the other hand, the higher the concentration of SA, the smoother the extrusion process, the flatter the filaments, making it more suitable for printing, which will be confirmed by the results of texture analysis.

In general, the printability of soybean protein-polysaccharide composite paste is aimed at printing out self-supporting, flat sample and smooth surface. To ensure printability, the ink should exhibit contrasting properties. Initially, it must be fluid enough to be pumped and extruded, yet it should also stiffen rapidly after deposition to enable construction. Therefore, the amount of different polysaccharides added is particularly important, and the range of proper mechanical properties should be between 900 Pa s and 1200 Pa s.

3.3. Texture profile analysis (TPA)

Texture profile analysis can detect several texture parameters, including hardness, springiness, adhesiveness, and others (Yuan et al., 2016). As shown in Table 2, paste samples without polysaccharides cannot determine the TPA parameters due to their extremely weak gel properties, highlighting the importance of incorporating polysaccharides in the ink for the production of self-supporting 3D printed food products. With an increase in polysaccharide concentration, the springiness, cohesiveness, gumminess, and resilience of the printed samples all significantly decreased (Table 2). This could be attributed to the changes in the repulsive forces between polysaccharide charges that affect molecular aggregation. Both carrageenan and sodium alginate are anionic polysaccharides that can form complexes with the amino group ($-NH_3^+$) of the protein through electrostatic interactions, thereby altering the printing characteristics of the paste (Huang et al., 2021). Sulfated polysaccharides such as carrageenan have the ability to interact with proteins above their isoelectric point. κC contains a sulfate group ($-OSO_3^-$) that can be bonded to the amino group ($-NH_3^+$) of the protein by electrostatic interaction. The electrostatic interaction between

sulfate group (- OSO_3^-) and protein is stronger than that between carboxyl group (-COO-) and protein (Huang et al., 2021). Furthermore, SPI possesses a globular structure, and the folded SPI structure can stretch and expose internal functional group structures upon heating, facilitating cross-linking with polysaccharide ions.

Hardness refers to the force required to compress a sample and can mimic the chewing behavior of the oral cavity on solids or semi-solids, serving as an indicator of the structural stability of 3D printed food. Compared to pastes with the same concentration of SA, the addition of κC significantly affects the properties, with an increase in sample hardness and a decrease in adhesiveness and springiness. When the κC concentration reached 2 wt%, high shear forces occur during the extrusion process, leading to filament breakage at the nozzle, resulting in poor shape fidelity and significant discrepancies between the printed samples and the intended model, making it also impossible to determine the TPA parameters. In contrast, the addition of SA, with the same concentration of κC, yields opposite results. This may be attributed to the disruption of the molecular chain structure of the samples during preparation, where longer polysaccharide chains exhibit stronger gelation properties with proteins (Monteiro & Lopes-da-Silva, 2017). The springiness of the samples refers to the physical reboundness after deformation, which can resist to external forces. At higher concentrations, polysaccharides dominate the springiness of the mixture, leading to a weakening of samples structure, as also reflected in the aforementioned rheological analysis (Warnakulasuriya & Nickerson, 2018). This is contrary to the experimental conclusion of (Xu et al.,2023). This result may be due to the fact that the sample has a hollow structure, and when the extrusion degree is 50%, the sample is forced to extrude from all sides to widen, resulting in a decrease in data presentation. Cohesiveness refers to the adhesive forces within the sample particles, reflecting the magnitude of intermolecular binding forces that allow the sample to maintain its integrity even under pressure. The data indicates that there is only a minor difference in cohesiveness between the samples, and the low concentration of polysaccharide improved the structural properties of the paste. When the concentration of polysaccharide was too high (>1.5%, wt %), the Cohesiveness and resilience of the sample decreased, which

was consistent with the results of (Xu et al.,2023). This may be attributed to changes in the repulsive forces between the negative charges in the polysaccharide, which affect molecular aggregation and thus alter the texture properties of the sample (Xu et al.,2023). The above results suggested a positive correlation between paste textural properties and polysaccharide concentration. Considering that plant-based foods are extruded with current inks as the main material, the protein paste having the formulations S15A1.5K1.5 exhibits optimal texture properties and is most suitable for 3D printing. In fact, the texture of plant-based foods largely depends on their structure, mechanical properties, and surface characteristics (Shi et al., 2023).

3.4. Microstructure

Figure 3 illustrates the microstructures of different ink formulations at various magnifications (1000×, 2500×, and 5000×). All food inks exhibit a heterogeneous microstructure composed of protein-polysaccharide particles forming aggregates. The structure of soybean isolate protein (SPI) has a rough surface because it is a paste at room temperature. However, the structural support provided by these concentrations is still insufficient to meet the required criteria, which may be the reason for the inability to achieve proper printability (Figure 1). Therefore, an appropriate polysaccharide concentration needs to be added to achieve gelation. Different ink formulations have different densification and orientation of the cavity, which is especially obvious after the addition of polysaccharides. Sodium alginate (SA) and kappa carrageenan (κC) bind strongly to protein particles, forming small fragmented block formations. SA, κC, and SPI particles form non-covalent bonds due to their hydrophilic nature and abundance of carboxyl and hydroxyl groups, which promote hydrophobic interactions and hydrogen bonding (Huang et al., 2021; Wei et al., 2023). As the κC content increased, the cross-linking structure with SPI-polysaccharide particles became rougher, resulting in a more disordered and chaotic ink system, forming large aggregates. This could be an increased interaction between κC and κC (Lu et al., 2022). This may explain why ink S15A1.5K1.5 was able to be extruded from the nozzle while ink S15A1.5K2 became clogged and ink S15A2K2 agglomerated (Figure 1). SA more ink formula surface is more compact and smoother, which is consistent with (Chen et al., 2022).

Overall, ink S15A1.5K1.5 has the best network density and can resist structural changes under high shear stress during the extrusion process.

3.5. Molecular interaction force analysis

As shown in Figure 4a, the solubility of the composite paste was significantly enhanced, indicating the presence of hydrophobic interactions, electrostatic interactions, disulfide bonds, and hydrogen bonds within the protein paste structure. The interaction forces between protein molecules and polysaccharides followed the order of hydrophobic interactions > electrostatic interactions > disulfide bond interactions > hydrogen bond interactions. This observation was consistent with the previously reported results (Lu et al., 2023). A slight decrease in electrostatic interactions was observed in the composite paste. This result can be attributed to the influence of negatively charged groups on the protein and polysaccharide surfaces, which are affected by the electrostatic binding under high polysaccharide concentrations, leading to conformational changes in the protein and exposing more hydrophobic groups (Wang et al., 2021). When electrostatic repulsion further increases, the distance between molecules becomes longer, making it difficult to detect the signal of electrostatic repulsion, resulting in decreased solubility. Compared to pure SPI paste, the addition of polysaccharides significantly increased hydrophobic interactions and hydrogen bond interactions in the paste ($p < 0.05$). This finding indicates that the addition of polysaccharides greatly enhances hydrophobic interactions and hydrogen bond interactions, playing a crucial role in the formation and maintenance of the SPI-polysaccharide paste system. This phenomenon may be attributed to the exposure of chemical groups within the protein matrix after thermal treatment. SA and κC are anionic acidic polysaccharides rich in carboxyl and hydroxyl groups. Although there is an intrinsic repulsion between them, but other forces can maintain the state without causing the system to separate, especially at high concentrations. Studies have shown that there is an electrostatic interaction between SPI and κC, where the negatively charged sulfate groups on κC can interact with the positively charged amino groups (-$OSO_3^-NH_3^+$) on proteins, even at pH above the isoelectric point (Huang et al., 2021; Lu et al., 2023). Additionally, SPI and polysaccharides can absorb moisture, promoting

498 further aggregation of proteins and overcoming the biocompatibility and inherent
499 repulsion between SPI and polysaccharides, ultimately forming a paste cross-linking
500 structure (Cao et al., 2022; Min et al., 2022).

501 **3.6. Composite paste forming mechanism**

502 Based on the intermolecular interactions and rheological properties discussed
503 above, this study presents a plausible hypothesis regarding the gelation mechanism of
504 SPI-polysaccharide (Figure 5). The experimental results revealed that hydrophobic
505 interactions and electrostatic interactions are the predominant forces in the composite
506 paste. Heating facilitates the exposure of hydrophobic groups in the protein, while the
507 polysaccharides SA and κC contain numerous carboxyl and hydroxyl groups,
508 enhancing hydrophobic interactions and hydrogen bonding with SPI particles (Huang
509 et al., 2021; Wei et al., 2023). The presence of a substantial number of hydrophobic
510 groups leads to protein crosslinking and aggregation. κC, on average, contains an
511 anionic sulfate group (- OSO_3^-) per disaccharide repeating unit, which can engage in
512 electrostatic interactions with cationic groups (-NH_3^+) of the protein. The electrostatic
513 interaction between sulfate group (- OSO_3^-) and protein is stronger than that between
514 carboxyl group (-COO-) and protein (Huang et al., 2021; Lu et al., 2023). In the SPI
515 system, the addition of κC forms protein-polysaccharide interactions, establishing a
516 balance between protein-protein and protein-polysaccharide interactions. This is
517 consistent with the fact that in all oscillation studies, the composite gel is visually
518 homogeneous and there is no phase separation. When the polysaccharide concentration
519 exceeds 1.5 wt%, the self-aggregation of polysaccharides hinders SPI cross-linking,
520 reducing its interaction with SPI. As the κC content increases, the κC -κC interaction
521 increases and the κC -protein interaction decreases, resulting in a stronger gel that is
522 unable to extrude from the nozzle. The molecular structure of SA is rich in hydroxyl
523 and carboxylic groups, and it is easy to form intermolecular hydrogen bonds with the
524 functional groups of other polymers (Wei et al., 2023). However, it has been reported
525 that SA alone exhibits inadequate mechanical properties in soft tissue engineering
526 applications, failing to provide sufficient mechanical support under stress conditions,
527 which aligns with our experimental results (Wei et al., 2023). But when the addition

amount of SA exceeds a certain critical value (2.5 wt%), it forms a gel with soybean protein, yielding improved printing performance. Some studies have successfully prepared alginate/carrageenan composite hydrogels with different concentrations of carrageenan, and bio-printed the alginate/carrageenan scaffold, the results show that the gel is suitable for using bioprinting to manufacture 3D hydrogel scaffold (Kim et al., 2019).

3.7. Fourier transform infrared (FTIR) analysis

In order to investigate the changes in chemical bonds in the inks, a comparison of their FTIR spectra was conducted, as shown in Figure 4b. The FTIR spectra of the paste samples did not exhibit any new peaks upon the addition of polysaccharides, and there were no new functional groups observed with varying ratios of SA and κC, indicating that the covalent interactions were minor. This is consistent with the research results of (Xing et al., 2024). All inks displayed a strong and broad absorption peak in the range of 3200-3600 cm^{-1}, which is typically associated with the stretching of O-H bonds and partially formed hydrogen bonds (Yu et al., 2022). Compared to the SPI 15, the O-H stretching bands of the ink with added polysaccharides shifted to lower wavenumbers. For instance, in the inks S15A2K1.5 and S15A2K2, the band of the SPI 15 ink at 3273 cm^{-1} shifted to 3282 cm^{-1} and 3286 cm^{-1}, respectively, suggesting stronger hydrogen bonding and increased molecular interactions in the S15A2K2 ink (Min et al., 2022). In fact, hydrogen bonding can form connections between proteins and polysaccharides, enhancing cross-linking strength, which is crucial for controlling the printability of different biomacromolecules in food inks (Warnakulasuriya & Nickerson, 2018). In all mixed pastes, weak peaks were also observed in the range of 2998-3018 cm^{-1}, which could be attributed to the stretching vibrations of C-H bonds (Min et al., 2022). Furthermore, all inks exhibited a peak at approximately 1633 cm^{-1}, which is related to the asymmetric and symmetric stretching of carboxylate groups (COO-) and has been suggested to be caused by the bending vibrations of water molecules (1650 cm^{-1}) (Hu et al., 2017; Shi et al., 2023). It is noteworthy that when different polysaccharides were added to SPI, all inks showed absorption peaks in the range of 1515-1531 cm^{-1}, with the bands shifting from higher to lower wavenumbers. These peaks are associated with

the amide I (1600–1700 cm^{-1}) and amide II (1500–1600 cm^{-1}) regions in the FT-IR spectra. The amide regions primarily represent the stretching vibrations of C=O, the bending vibrations of N-H, and the stretching vibrations of C-N, which are reliable indicators of protein secondary structure conformation (Carbonaro & Nucara, 2010). The shift of bands from higher to lower wavenumbers indicates a decrease in the content of α-helical structures and an increase in the proportion of β-sheet structures in the paste (Liu et al., 2022). The results demonstrate that the combination of polysaccharides and SPI significantly alters the spatial structure of the paste.

3.8. X-ray diffraction (XRD) analysis

The X-ray diffraction patterns can be used to determine the amorphous or crystalline nature of molecules (Dong et al., 2021). As shown in Figure 4c, SPI exhibits two sharp peaks at diffraction angles of 9° and 19°, indicating its crystalline structure. Its primary structure is believed to consist of an α-helical and β-sheet structure (Chen et al., 2013; Dong et al., 2021). In contrast, the addition of polysaccharides to the composite paste results in two relatively flat peaks around 9°, suggesting a significant reduction in the α-helical structure and a presumed transition to the β-sheet structure. This also indicates the formation of amorphous complexes between SPI and polysaccharide molecules. Such amorphous nature is directly related to the hydrophilicity and hygroscopicity of the polymer (Wang et al., 2018). Composite pastes prepared with formulations S15A1.5K1.5 and S15A1.5K2 exhibit broad diffraction peaks at approximately 19°, while formulations S15A2K1.5 and S15A2K2 show increased peak intensities and sharpened peaks. These structural changes suggested a corresponding interplay between the α-helical and β-sheet structures, with an increase in SA concentration potentially leading to the transformation of the α-helical structure to the β-sheet structure in the paste samples (Pan et al., 2022). It has been found that β-sheet structures have greater potential energy compared to α-helices, which can explain why the composite paste exhibits a more stable structure than the SPI paste (Ding et al., 2003). When the SA concentration is 1.5 wt%, the peak intensity of the composite paste significantly weakens. This indicates good compatibility between the two polymers (Y. Dong et al., 2021). At an SA concentration of 2 wt%, the peak intensity increases and

becomes sharper around 19°, indicating the formation of amorphous complexes and intermolecular interactions. These results demonstrated that the presence of κC and SA influences the crystallinity of the SPI paste system making it promising for 3D printing.

3.9. Differential scanning calorimetry (DSC) analysis

The properties and structure of most substances vary with temperature, and therefore, the stability of the sample structure can be reflected by the changes in endothermic and exothermic behavior in the DSC spectra. The enthalpy change and transition temperature can be determined based on the temperature and peak area corresponding to the largest peak in the graph (Hou et al., 2022). The influence of different polysaccharide concentrations on the thermal stability of the composite paste is shown in Figure 4d. The addition of the polysaccharides significantly affects the thermal transition temperature, resulting in an upward shift of the melting temperature from 89.6 °C to higher temperatures as the polysaccharide content increases. The melting temperatures for S15A1.5K1.5, S15A1.5K2, S15A2K1.5, and S15A2K2 are 95.3 °C, 92.8 °C, 93.5 °C, and 95.2 °C, respectively. This can be attributed to the interaction between the amino and carboxyl groups of SPI and the hydroxyl groups of the polysaccharides through hydrogen bonding, consistent with the aforementioned intermolecular forces. As the polysaccharide quantity increases, the melting temperature of the composite paste gradually rises, indicating a higher amount of heat absorbed during the sample melting process and an enhancement in thermal stability. Within the melting temperature range, SA and κC in the composite paste may form a cross-linked structure, with some SPI potentially participating in the formation of the structure and being encapsulated within it. This promotes the stability of the dense cross-linking system, ultimately leading to changes in thermal stability. These findings suggest a certain degree of interaction between SPI and polysaccharides, resulting in a covalently cross-linked composite paste system, which could explain the paste's elasticity, viscosity, and strength.

4. Conclusion

In this study, a 3D printable ink was prepared using soy protein isolate, carrageenan, and sodium alginate. The addition of polysaccharides to soy protein at

appropriate concentrations facilitated the interaction between proteins and polysaccharides, resulting in protein-polysaccharide pastes with optimal 3D printing quality. This combination provides a viable method for the production innovative of plant-based foods. Rheological and textural analyses revealed that the addition of polysaccharides increased the viscosity and hardness of the printing ink. The S15A1.5K1.5 ink exhibited favorable viscosity and storage modulus (G'), enabling stable printability. FT-IR analysis and molecular interaction within the dense cross-linking indicated that the introduction of polysaccharides led to the formation of hydrogen bonds through the -OH groups, transforming α-helices into β-sheets. Hydrophobic interactions, electrostatic interactions, and disulfide bonding were identified as the main driving forces maintaining the paste structure. SEM images displayed the rough surface of the composite material, confirming the formation of a dense cross-linking structure between SPI and polysaccharides. XRD results indicated that the interactions between SPI and polysaccharides led to a transition from a crystalline to an amorphous structure. DSC analysis demonstrated that the addition of polysaccharides significantly enhanced the thermal stability of the composite paste. These findings contribute to the improvement of texture and quality in protein-polysaccharide pastes, as well as the practical application of 3D printing technology in plant-based food, establishing both theoretical and practical foundations. In our next studies, we will explore various ink formulations using other types of food ingredients, such as pea protein isolate, to meet specific nutritional requirements of individuals.

Acknowledgements

This work was supported by the Key Research and Development Projects of Zhejiang [grant numbers 2022C04021, 2022C02041]; the Zhejiang Provincial Natural Science Foundation [grant number LQ23C200013].

References

Bi, C.-h., Zhu, Y.-d., Li, L.-t., Zhang, Y.-l., Hua, Z., Zhu, J.-y., Liu, Y., Liu, Y.-d., & Huang, Z.-g. (2018). Rheological properties and microstructure of soy protein isolate /κ-carrageenan gels under high-speed shear treatment. *Journal of Food Engineering, 236*, 44-50. https://doi.org/10.1016/j.jfoodeng.2018.05.006

Cao, J., Tong, X., Wang, M., Tian, T., Yang, S., Sun, M., Lyu, B., Cao, X., Wang, H., & Jiang, L. (2022). Soy Protein Isolate/Sodium Alginate Microparticles under Different pH Conditions: Formation Mechanism and Physicochemical Properties. *Foods, 11*(6), 790. https://doi.org/10.3390/foods11060790

Carbonaro, M., & Nucara, A. (2010). Secondary structure of food proteins by Fourier transform spectroscopy in the mid-infrared region. *Amino Acids, 38*(3), 679-690. https://doi.org/10.1007/s00726-009-0274-3

Chen, Jingwang, Mu, T., Goffin, D., Blecker, C., Richard, G., Richel, A., & Haubruge, E. (2019). Application of soy protein isolate and hydrocolloids based mixtures as promising food material in 3D food printing. *Journal of Food Engineering, 261*, 76-86. https://doi.org/10.1016/j.jfoodeng.2019.03.016

Chen, Jingwang, Sun, H., Mu, T., Blecker, C., Richel, A., Richard, G., Jacquet, N., Haubruge, E., & Goffin, D. (2022). Effect of temperature on rheological, structural, and textural properties of soy protein isolate pastes for 3D food printing. *Journal of Food Engineering, 323*, 110917. https://doi.org/10.1016/j.jfoodeng.2021.110917

Chen, Jun, Chen, X., Zhu, Q., Chen, F., Zhao, X., & Ao, Q. (2013). Determination of the domain structure of the 7S and 11S globulins from soy proteins by XRD and FTIR. *Journal of the Science of Food and Agriculture*, *93*(7), 1687-1691. https://doi.org/10.1002/jsfa.5950

Cheng, Y., Fu, Y., Ma, L., Yap, P. L., Losic, D., Wang, H., & Zhang, Y. (2022). Rheology of edible food inks from 2D/3D/4D printing, and its role in future 5D/6D printing. *Food Hydrocolloids*, *132*, 107855. https://doi.org/10.1016/j.foodhyd.2022.107855

Dankar, I., Haddarah, A., Omar, F. E. L., Sepulcre, F., & Pujolà, M. (2018). 3D printing technology: The new era for food customization and elaboration. *Trends in Food Science & Technology*, *75*, 231-242. https://doi.org/10.1016/j.tifs.2018.03.018

Dick, A., Bhandari, B., Dong, X., & Prakash, S. (2020). Feasibility study of hydrocolloid incorporated 3D printed pork as dysphagia food. *Food Hydrocolloids*, *107*, 105940. https://doi.org/10.1016/j.foodhyd.2020.105940

Ding, F., Borreguero, J. M., Buldyrey, S. V., Stanley, H. E., & Dokholyan, N. V. (2003). Mechanism for the α-helix to β-hairpin transition. *Proteins: Structure, Function, and Bioinformatics*, *53*(2), 220-228. https://doi.org/10.1002/prot.10468

Dong, Die, & Cui, B. (2021). Fabrication, characterization and emulsifying properties of potato starch/soy protein complexes in acidic conditions. *Food Hydrocolloids*, *115*, 106600. https://doi.org/10.1016/j.foodhyd.2021.106600

Dong, Y., Huang, Z., Niu, L., & Xiao, J. (2021). Influence of kappa-carrageenan on the gel properties of auricularia auricular-judae during freeze–thaw cycles. *International Journal of Food Science & Technology*, *56*(2), 1048-1060. https://doi.org/10.1111/ijfs.14760

Dorishetty, P., Balu, R., Sreekumar, A., de Campo, L., Mata, J. P., Choudhury, N. R., & Dutta, N. K. (2019). Robust and Tunable Hybrid Hydrogels from Photo-Cross-Linked Soy Protein Isolate and Regenerated Silk Fibroin. *ACS Sustainable Chemistry & Engineering*, *7*(10), 9257-9271.

10.1021/acssuschemeng.9b00147

Fernández Farrés, I., Douaire, M., & Norton, I. T. (2013). Rheology and tribological properties of Ca-alginate fluid gels produced by diffusion-controlled method. *Food Hydrocolloids*, *32*(1), 115-122. https://doi.org/10.1016/j.foodhyd.2012.12.009

Fu, Z., Naghieh, S., Xu, C., Wang, C., Sun, W., & Chen, X. (2021). Printability in extrusion bioprinting. *Biofabrication*, *13*(3), 033001. https://doi.org/10.1088/1758-5090/abe7ab

Hou, Y., Liu, H., Zhu, D., Liu, J., Zhang, C., Li, C., & Han, J. (2022). Influence of Soybean Dietary Fiber on the properties of Konjac Glucomannan/κ-Carrageenan Corn Oil Composite Gel. *Food Hydrocolloids*, *129*, 107602. https://doi.org/10.1016/j.foodhyd.2022.107602

Hu, B., Chen, Q., Cai, Q., Fan, Y., Wilde, P. J., Rong, Z., & Zeng, X. (2017). Gelation of soybean protein and polysaccharides delays digestion. *Food Chemistry*, *221*, 1598-1605. https://doi.org/10.1016/j.foodchem.2016.10.132

Huang, M., Mao, Y., Li, H., & Yang, H. (2021). Kappa-carrageenan enhances the gelation and structural changes of egg yolk via electrostatic interactions with yolk protein. *Food Chemistry*, *360*, 129972. https://doi.org/10.1016/j.foodchem.2021.129972

Jiang, H., Zheng, L., Zou, Y., Tong, Z., Han, S., & Wang, S. (2019). 3D food printing: main components selection by considering rheological properties. *Critical reviews in food science and nutrition*, *59*(14), 2335-2347. https://doi.org/10.1080/10408398.2018.1514363

Keerthana, K., Anukiruthika, T., Moses, J. A., & Anandharamakrishnan, C. (2020). Development of fiber-enriched 3D printed snacks from alternative foods: A study on button mushroom. *Journal of Food Engineering*, *287*, 110116. https://doi.org/10.1016/j.jfoodeng.2020.110116

Kim, M. H., Lee, Y. W., Jung, W.-K., Oh, J., & Nam, S. Y. (2019). Enhanced rheological behaviors of alginate hydrogels with carrageenan for extrusion-based bioprinting. *Journal of the Mechanical Behavior of Biomedical Materials*, *98*, 187-194. https://doi.org/10.1016/j.jmbbm.2019.06.014

Liu, Z., Bhandari, B., Prakash, S., Mantihal, S., & Zhang, M. (2019). Linking rheology and printability of a multicomponent gel system of carrageenan-xanthan-starch in extrusion based additive manufacturing. *Food Hydrocolloids*, *87*, 413-424. https://doi.org/10.1016/j.foodhyd.2018.08.026

Liu, Z., Xing, X., Xu, D., Chitrakar, B., Hu, L., Hati, S., Mo, H., & Li, H. (2022). Correlating rheology with 3D printing performance based on thermo-responsive κ-carrageenan/Pleurotus ostreatus protein with regard to interaction mechanism. *Food Hydrocolloids*, *131*, 107813. https://doi.org/10.1016/j.foodhyd.2022.107813

Lopez Hernandez, H., Souza, J. W., & Appel, E. A. (2021). A Quantitative Description for Designing the Extrudability of Shear-Thinning Physical Hydrogels. *Macromolecular Bioscience*, *21*(2), 2000295. https://doi.org/10.1002/mabi.202000295

Lu, Z., Lee, P.-R., & Yang, H. (2022). Chickpea flour and soy protein isolate interacted with κ-carrageenan via electrostatic interactions to form egg omelets analogue. *Food Hydrocolloids*, *130*, 107691. https://doi.org/10.1016/j.foodhyd.2022.107691

Lu, Z., Lee, P.-R., & Yang, H. (2023). Kappa-carrageenan improves the gelation and structures of soy protein isolate through the formation of hydrogen bonding and electrostatic interactions. *Food Hydrocolloids*, *140*, 108585. https://doi.org/10.1016/j.foodhyd.2023.108585

Min, C., Ma, W., Kuang, J., Huang, J., & Xiong, Y. L. (2022). Textural properties, microstructure and digestibility of mungbean starch–flaxseed protein composite gels. *Food Hydrocolloids*, *126*, 107482. https://doi.org/10.1016/j.foodhyd.2022.107482

Monteiro, S. R., & Lopes-da-Silva, J. A. (2017). Effect of the molecular weight of a neutral polysaccharide on soy protein gelation. *Food Research International*, *102*, 14-24. https://doi.org/10.1016/j.foodres.2017.09.066

Osi, A. R., Zhang, H., Chen, J., Zhou, Y., Wang, R., Fu, J., Müller-Buschbaum, P., & Zhong, Q. (2021). Three-Dimensional-Printable Thermo/Photo-Cross-Linked Methacrylated Chitosan−Gelatin Hydrogel Composites for Tissue Engineering. *ACS Applied Materials & Interfaces*, *13*(19), 22902-22913. https://doi.org/10.1021/acsami.1c01321

Pan, H., Pei, F., Ma, G., Ma, N., Zhong, L., Zhao, L., & Hu, Q. (2022). 3D printing properties of Flammulina velutipes polysaccharide-soy protein complex hydrogels. *Journal of Food Engineering*, *334*, 111170. https://doi.org/10.1016/j.jfoodeng.2022.111170

Phuhongsung, P., Zhang, M., & Devahastin, S. (2020). Investigation on 3D printing ability of soybean protein isolate gels and correlations with their rheological and textural properties via LF-NMR spectroscopic characteristics. *Lwt*, *122*, 109019. https://doi.org/10.1016/j.lwt.2020.109019

Qin, X.-S., Chen, S.-S., Li, X.-J., Luo, S.-Z., Zhong, X.-Y., Jiang, S.-T., Zhao, Y.-Y., & Zheng, Z. (2017). Gelation Properties of Transglutaminase-Induced Soy Protein Isolate and Wheat Gluten Mixture with Ultrahigh Pressure Pretreatment. *Food and Bioprocess Technology*, *10*(5), 866-874. https://doi.org/10.1007/s11947-017-1864-9

Rowat, S. J. A., Legge, R. L., & Moresoli, C. (2021). Plant protein in material extrusion 3D printing: Formation, plasticization, prospects, and challenges. *Journal of Food Engineering*, *308*, 110623. https://doi.org/10.1016/j.jfoodeng.2021.110623

Shi, H., Li, J., Xu, E., Yang, H., Liu, D., & Yin, J. (2023). Microscale 3D printing of fish analogues using soy protein food ink. *Journal of Food Engineering*, *347*, 111436. https://doi.org/10.1016/j.jfoodeng.2023.111436

Wang, Wenjie, Shen, M., Jiang, L., Song, Q., Liu, S., & Xie, J. (2020). Influence of Mesona blumes polysaccharide on the gel properties and microstructure of acid-induced soy protein isolate gels. *Food Chemistry*, *313*, 126125. https://doi.org/10.1016/j.foodchem.2019.126125

Wang, Wenjie, Shen, M., Liu, S., Jiang, L., Song, Q., & Xie, J. (2018). Gel properties and interactions of Mesona blumes polysaccharide-soy protein isolates mixed gel: The effect of salt addition. *Carbohydrate Polymers*, *192*, 193-201. https://doi.org/10.1016/j.carbpol.2018.03.064

Wang, Ya-Ru, Yang, Q., Li-Sha, Y.-J., & Chen, H.-Q. (2021). Structural, gelation properties and microstructure of rice glutelin/sugar beet pectin composite gels: Effects of ionic strengths. *Food Chemistry*, *346*, 128956. https://doi.org/10.1016/j.foodchem.2020.128956

Warnakulasuriya, S. N., & Nickerson, M. T. (2018). Review on plant protein–polysaccharide complex coacervation, and the functionality and applicability of formed complexes. *Journal of the Science of Food and Agriculture*, *98*(15), 5559-5571. https://doi.org/10.1002/jsfa.9228

Warner, E. L., Norton, I. T., & Mills, T. B. (2019). Comparing the viscoelastic properties of gelatin and different concentrations of kappa-carrageenan mixtures for additive manufacturing applications. *Journal of Food Engineering*, *246*, 58-66. https://doi.org/10.1016/j.jfoodeng.2018.10.033

Wei, Q., Zhou, J., An, Y., Li, M., Zhang, J., & Yang, S. (2023). Modification, 3D printing process and application of sodium alginate based hydrogels in soft tissue engineering: A review. *International Journal of Biological Macromolecules*, *232*, 123450. https://doi.org/10.1016/j.ijbiomac.2023.123450

Xie, R., Mukherjee, S., Levi, A. E., Reynolds, V. G., Wang, H., Chabinyc, M. L., & Bates, C. M. (2020).

Room temperature 3D printing of super-soft and solvent-free elastomers. *Science Advances*, *6*(46), eabc6900. 10.1126/sciadv.abc6900

Xing, H., Liu, X., Hu, Y., Hu, K., & Chen, J. (2024). Effect of Lycium barbarum polysaccharides on heat-induced gelation of soy protein isolate. *Food Hydrocolloids*, *147*, 109323. https://doi.org/10.1016/j.foodhyd.2023.109323

Xu, K., Wu, C., Fan, G., Kou, X., Li, X., Li, T., Dou, J., & Zhou, Y. (2023). Rheological properties, gel properties and 3D printing performance of soy protein isolate gel inks added with different types of apricot polysaccharides. *International Journal of Biological Macromolecules*, *242*, 124624. https://doi.org/10.1016/j.ijbiomac.2023.124624

Yang, F., Zhang, M., Bhandari, B., & Liu, Y. (2018). Investigation on lemon juice gel as food material for 3D printing and optimization of printing parameters. *Lwt*, *87*, 67-76. https://doi.org/10.1016/j.lwt.2017.08.054

Yu, J., Wang, X.-y., Li, D., Wang, L.-j., & Wang, Y. (2022). Development of soy protein isolate emulsion gels as extrusion-based 3D food printing inks: Effect of polysaccharides incorporation. *Food Hydrocolloids*, *131*, 107824. https://doi.org/10.1016/j.foodhyd.2022.107824

Yuan, C., Du, L., Zhang, G., Jin, Z., & Liu, H. (2016). Influence of cyclodextrins on texture behavior and freeze-thaw stability of kappa-carrageenan gel. *Food Chemistry*, *210*, 600-605. https://doi.org/10.1016/j.foodchem.2016.05.014

Zhang, C., Wang, C.-S., Therriault, D., & Heuzey, M.-C. (2022). Development of aqueous protein/polysaccharide mixture-based inks for 3D printing towards food applications. *Food Hydrocolloids*, *131*, 107742. https://doi.org/10.1016/j.foodhyd.2022.107742

Table captions

Table 1. Composition of different 3D printing ink formulations (wt%).

Table 2. Texture profile analysis (TPA) indicators for different 3D printed pastes with different formulations.

804 **Table 1**. Composition of different 3D printing ink formulations (wt%).

Inks	Water/(ml)	SPI/(g)	SA/(g)	κC /(g)
SPI 15	85	15	-	-
S15A1K1	85	15	1.0	1.0
S15A1K1.5	85	15	1.0	1.5
S15A1.5K1	85	15	1.5	1.0
S15A1.5K1.5	85	15	1.5	1.5
S15A1.5K2	85	15	1.5	2.0
S15A2K1.5	85	15	2.0	1.5
S15A2K2	85	15	2.0	2.0

805 In the codes listed for formulation column, S15AmKn food ink means that SPI, SA, and κC
806 constitute 15 wt%, m wt% and n wt%, respectively.

807

Table 2. Texture profile analysis (TPA) indicators for different 3D printed pastes with different formulations.

Sample	Hardness (g)	Adhesiveness	Springiness	Cohesiveness	Gumminess	Chewiness	Resilience (g•sec)
SPI 15	-	-	-	-	-	-	-
S15A1K1	529.27±14.13 ^{a}	-7.22±3.31 ^{a}	0.78±0.02 ^{a}	0.42±0.03 ^{a}	223.55±19.90 ^{a}	173.18±13.32 ^{a}	0.17±0.01 ^{a}
S15A1K1.5	552.91±20.28 ^{a}	-23.60±2.73 ^{c}	0.46±0.02 ^{c}	0.37±0.01 ^{b}	205.01±2.26 ^{b}	94.93±4.41 ^{b}	0.11±0.01 ^{b}
S15A1.5K1	480.10±8.76 ^{b}	-14.14±3.39 ^{b}	0.59±0.02 ^{b}	0.36±0.01 ^{bc}	172.20±4.56 ^{c}	101.65±5.83 ^{b}	0.11±0.01 ^{b}
S15A1.5K1.5	538.73±12.16 ^{a}	-56.24±1.93 ^{e}	0.45±0.02 ^{c}	0.33±0.01 ^{c}	180.06±7.39 ^{c}	81.88±2.62 ^{c}	0.08±0.00 ^{d}
S15A1.5K2	-	-	-	-	-	-	-
S15A2K1.5	429.84±7.18 ^{c}	-43.74±3.38 ^{d}	0.45±0.01 ^{c}	0.35±0.00 ^{bc}	150.22±2.08 ^{d}	67.47±0.47 ^{d}	0.10±0.00 ^{c}
S15A2K2	-	-	-	-	-	-	-

Values were expressed as the mean ± standard deviation (n = 3). Different letters indicated significant differences ($p < 0.05$) between values in the same column. "-" means not shaped. S15AmKn food ink means that SPI, SA, and κC constitute 15 wt%, m wt% and n wt%, respectively.

Figure captions

Figure 1. Analysis of 3D printing of different ink formulations and pictures of the printed products.

Figure 2. Rheological properties analysis of different ink formulations: (a): viscosity; (b): strain provide information which lines for G′ and G″; (c): storage modulus G′; (d): loss modulus G″.

Figure 3. Microstructure of ink formulations with different magnifications of 1000 ×, 2500 × and 5000 ×.

Figure 4. (a): Changes in molecular interaction force of the composite pastes in the presence of different polysaccharide concentrations. Mean values with different letters (a-d) differ significantly ($p < 0.05$); (b): The Fourier transform infrared, (FTIR) spectrum characterization, (c): X-ray diffractograms and (d): DSC thermograms of composite pastes with different formulations.

Figure 5. The formation mechanism diagram of SPI-polysaccharide composite pastes.

Figure 1

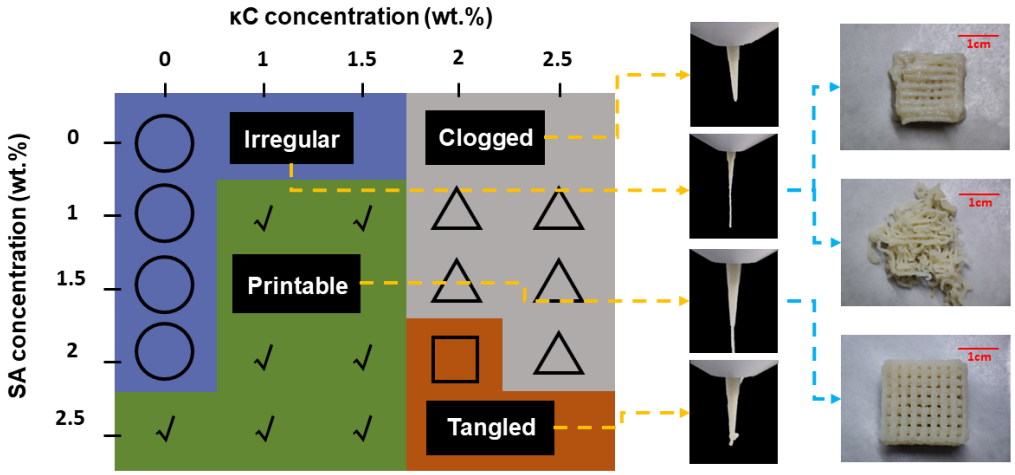

Figure 1. Analysis of 3D printing of different ink formulations and pictures of the printed products.

835 **Figure 2**

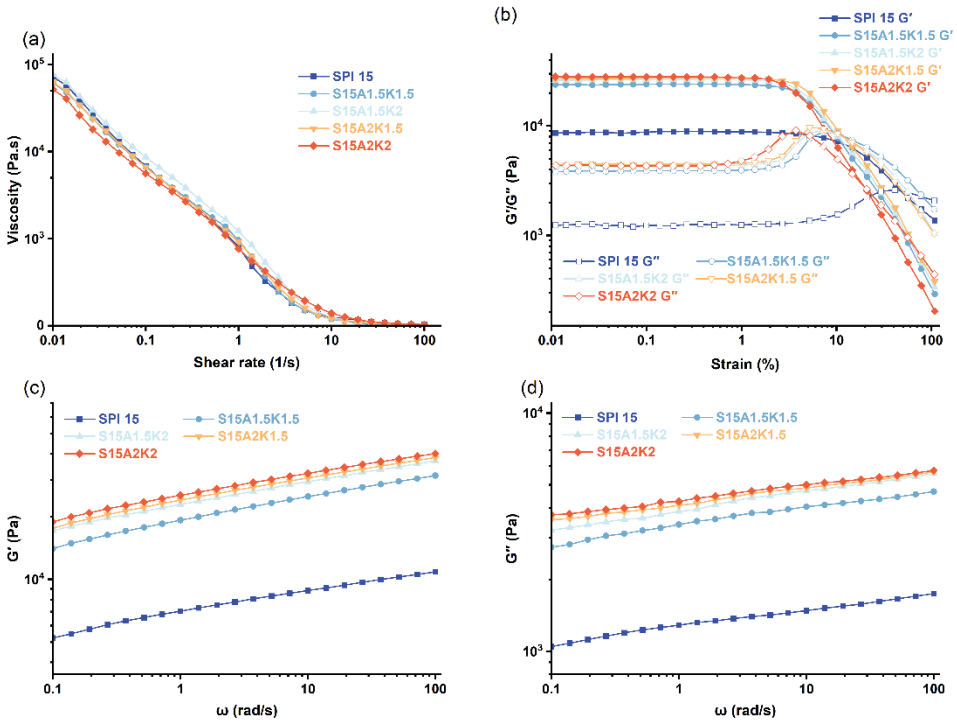

836

837 Figure 2. Rheological properties analysis of different ink formulations: (a): viscosity;

838 (b): strain provide information which lines for G′ and G″; (c): storage modulus G′; (d):

839 loss modulus G″.

840

841 **Figure 3**

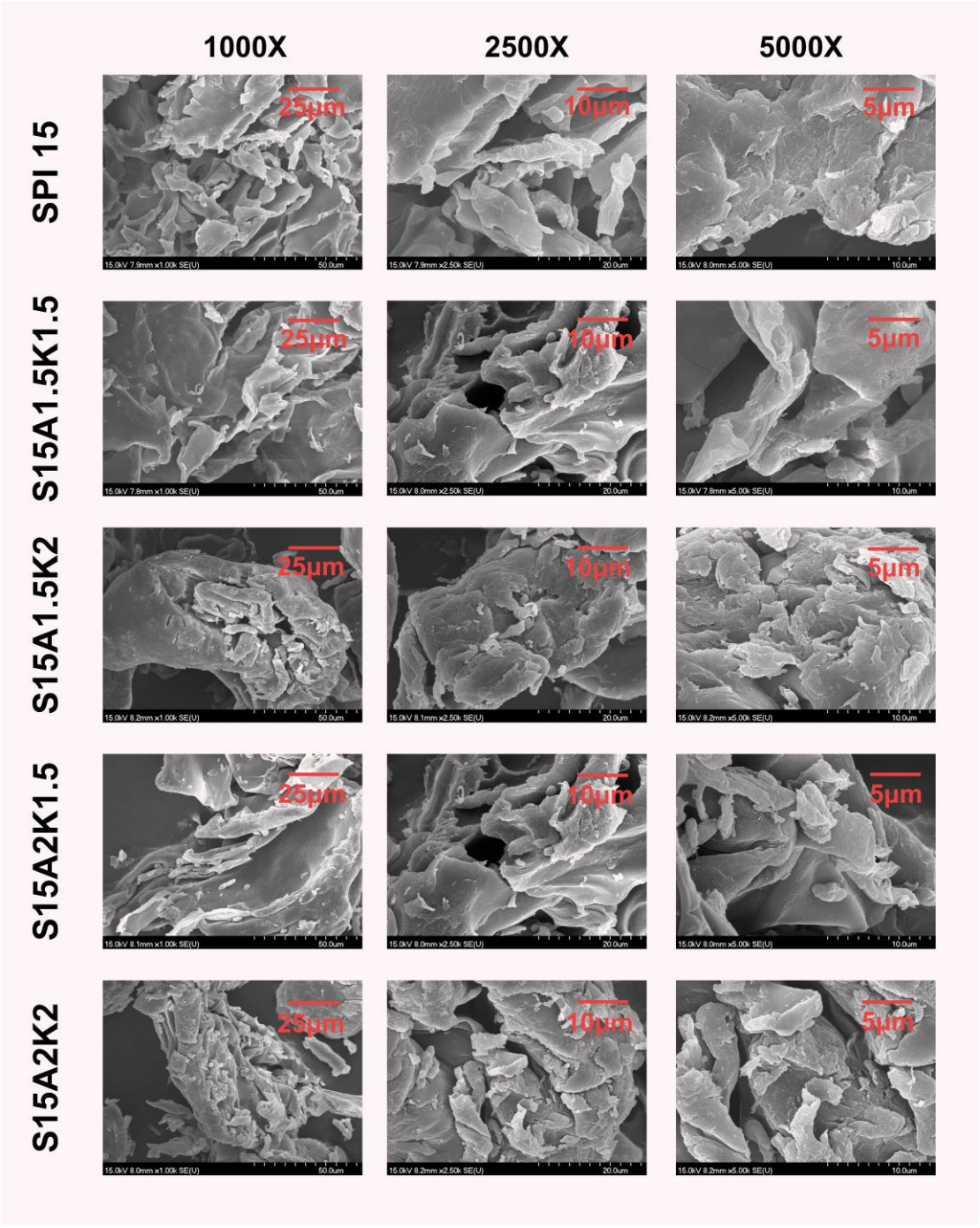

842

843 Figure 3. Microstructure of ink formulations with different magnifications of 1000 ×,

844 2500 × and 5000 ×.

845

Figure 4

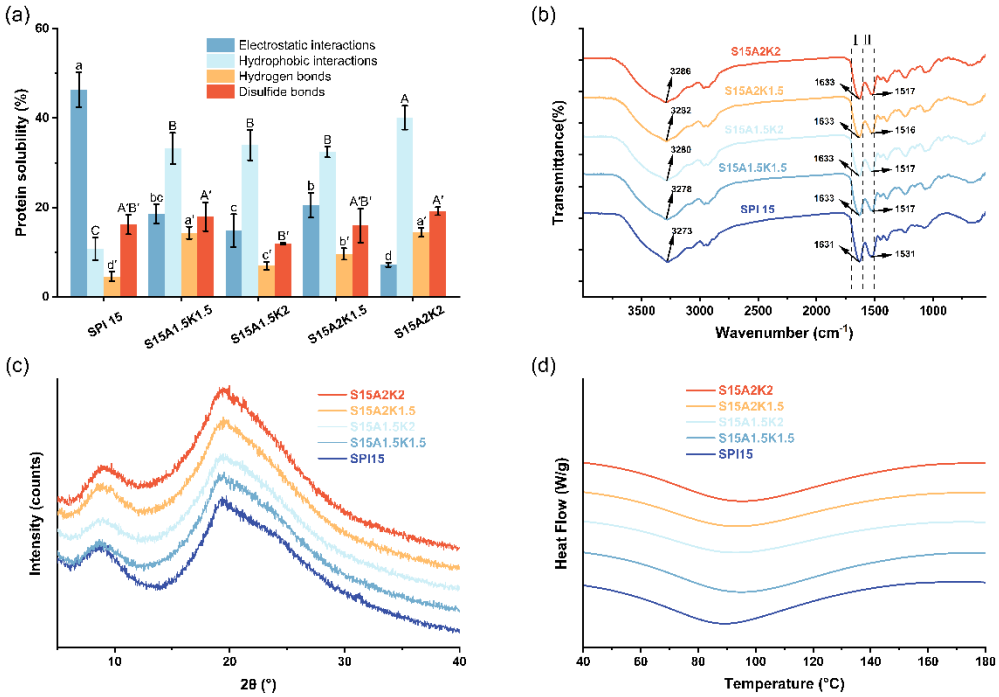

Figure 4. (a): Changes in molecular interaction force of the composite pastes in the presence of different polysaccharide concentrations. Mean values with different letters (a-d) differ significantly ($p < 0.05$); (b): The Fourier transform infrared, (FTIR) spectrum characterization; (c): X-ray diffractograms and (d): DSC thermograms of composite pastes with different formulations.

853 **Figure 5**

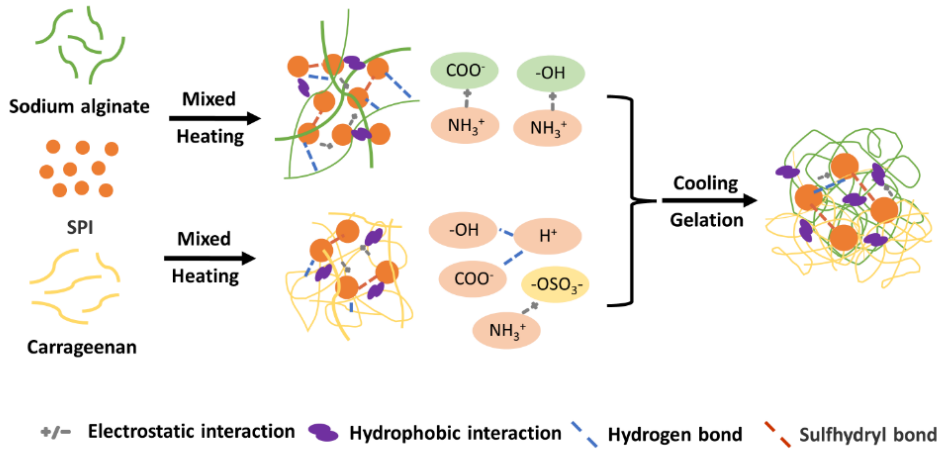

854 Figure 5. The formation mechanism diagram of SPI-polysaccharide composite pastes.

The authors declared that they have no conflicts of interest to this work. We declare that we do not have any commercial or associative interest that represents a conflict of interest in connection with the work submitted.

Author Contributions

Jian Wang: Conceptualization, Methodology, Writing - Review & Editing, Funding acquisition. Quanjin Jiang: Investigation, Data curation, Software, Writing - Original draft preparation. Zhenyu Huang: Visualization, Methodology, Investigation. Ahsan Hafiz Muhammad: Writing - Reviewing and Editing. Adem Gharsallaoui: Writing - Reviewing and Editing. Ming Cai: Supervision, Funding acquisition. Kai Yang: Supervision, Funding acquisition. Peilong Sun: Supervision, Project administration.

Rheological and mechanical behavior of soy protein-polysaccharide composite paste for extrusion-based 3D food printing: effects of type and concentration of polysaccharides

Jian Wang [a b †], Quanjin Jiang [a †], Zhenyu Huang [a], Ahsan Hafiz Muhammad [a], Adem Gharsallaoui [c], Ming Cai [a b *], Kai Yang [a b *], Peilong Sun [a b *]

[a] College of Food Science and Engineering, Zhejiang University of Technology, Chaowang 18, Hangzhou 310014, Zhejiang, China

[b] Key Laboratory of Food Macromolecular Resources Processing Technology Research (Zhejiang University of Technology), China National Light Industry, Hangzhou 310014, Zhejiang, China

[c] CNRS, LAGEPP UMR 5007, Univ. Lyon, University Claude Bernard Lyon 1, 43 Bd 11 Novembre 1918, Villeurbanne, 69622, Lyon, France

[*] Corresponding authors: caiming@zjut.edu.cn (M.C.); yangkai@zjut.edu.cn (K.Y.); sun_pl@zjut.edu.cn (P.S.); Tel.: +86-0571-88813775; Fax.: +86-0571-88813778.

[†] These authors contributed equally to this work.

Abstract

Soy protein isolate (SPI)-based pastes are widely employed for 3D printing of food materials. However, their rheological properties often do not meet the 3D printing requirements. To enhance the 3D printing characteristics of SPI pastes, this study combined SPI with carrageenan and sodium alginate to form composite materials. The effect of polysaccharide type and concentration on the rheological and textural properties of the ink was investigated to elucidate the mechanism of interaction between proteins and polysaccharides. The results demonstrated that the addition of carrageenan (1.5%, wt %) and sodium alginate (1.5%, wt %) effectively improved the mechanical properties of the paste, such as hardness and adhesiveness, enhanced thus the quality of 3D printed products. With the increase of polysaccharide proportion, the apparent viscosity and storage modulus (G') of the composite paste increased significantly. Fourier-transform infrared spectroscopy (FT-IR), protein solubility measurement, X-ray diffraction (XRD), and differential scanning calorimetry (DSC) were employed and the results revealed notable interactions among SPI and two kinds of polysaccharides, with electrostatic interactions and hydrophobic interactions being the primary driving forces. The addition of polysaccharides induced changes in the paste crystalline state and improved its thermal stability. Scanning electron microscopy (SEM) confirmed a uniform and compact microstructure due to the incorporation of polysaccharides. Consequently, the SPI-polysaccharide paste can be considered as novel material for 3D printing food materials, and the results of this study provides a theoretical foundation for its application in the field of plant-based food products.

Keywords: 3D printing; SPI-polysaccharide composite paste; Printability; Rheological properties

1. Introduction

3D printing is an efficient and convenient processing technology. Because of its bottom-up stacking approach, can print and manufacture complex and complicated structures that traditional processing methods cannot construct (Dankar et al., 2018). It has broad applications in various fields such as textiles, architecture, healthcare, and food (Keerthana et al., 2020). 3D food printing is revolutionizing the food processing industry by creating novel foods with complex shapes, distinctive textures, and enhanced nutritional value. This allows for personalized nutrition and customized food design, catering to the specific needs of aging populations, children, and sick patients. (Phuhongsung et al., 2020). Typically, extrusion, binder jetting, and inkjet printing technologies have been explored for various 3D food printing applications (Cheng et al., 2022). Among them, extrusion-based printing technique can be effectively used for semi-solid pastes such as grain dough, meat puree, and chocolate. The principle of this technique is to extrude material layer by layer through a nozzle to form a complex 3D structure (Rowat et al., 2021). Extrusion technology is currently the most widely studied method for 3D food printing. The emergence of 3D food printing technology helps to accelerate the development of new food products and become a potential technological mean to rebuild the conventional food supply chain (Chen et al., 2019).

Proteins and polysaccharides are two essential nutrients in the human food system that can alter their structural and functional properties, such as the ability to form gels or emulsions, through electrostatic forces and hydrogen bonds (Zhang et al., 2022). Soy protein isolate (SPI) as a food component has been widely used in 3D printing (Chen et al., 2019; Phuhongsung et al., 2020). However, SPI exhibits limitations in terms of printing accuracy and stability, as it is prone to breakage under high shearing forces. To address this issue, the addition of hydrocolloids or salt ions to SPI has been identified as a viable solution (Xu et al., 2023). Previous research has demonstrated the effectiveness of incorporating apricot polysaccharide into SPI, resulting in improved gelatinization performance and viscoelasticity of the SPI gel (Xu et al., 2023). Polysaccharide is a kind of natural macromolecular carbohydrate with complex and huge molecular structure obtained from multiple monosaccharides after dehydration

and condensation. Although polysaccharides are widely distributed in nature, not all polysaccharides are called food polysaccharides. Food polysaccharide refers to the polysaccharide that is allowed as a food additive in the food processing process to control the sensory quality, physical properties and improve the nutritional value of food. Kappa-Carrageenan (κC), a widely used polysaccharide in the food industry, exhibits rapid thermal-reversible behavior and can form robust and brittle gel structures suitable for 3D printing (Liu et al., 2019; Yu et al., 2022). Additionally, alginates are widely used as 3D printing materials because of their good gelling properties due to their many carboxyl and hydroxyl groups (Chen et al., 2019). Dick et al. (2020) investigated the effects of different ink polysaccharides on the rheology and texture of pig meat and found that the addition of ink polysaccharides improved the printability and texture of the meat. Studies have reported that SPI mixed with sodium alginate and gelatin as a 3D printing material improved the hardness and chewiness of 3D printed geometries, and SPI paste will be a promising material for 3D food printing (Chen et al., 2019).

Currently, 3D printing of food is still in its early stages. Warner et al. (2019) investigated the 3D printability of a mixture of gelatin and κC and found that the addition of κC resulted in a more stable structure than pure gelatin. Commercially, the 3D printed plant-based beef product “Alt Steak” produced by Israeli startup Redefine Meat has been sold in over 120 restaurants in Israel, the Netherlands, Germany, and the United Kingdom. Japanese company “Open Meals” uses 3D printer to print edible pixelated sushi. Each sushi is composed of edible gel with specific color and taste. However, to date, there has been limited exploration of 3D printing of SPI-polysaccharide composite pastes. At the same time, carrageenan and sodium alginate are extracted from plants, and we consider maintaining a plant-based property in the material properties of the ink, which can be used as a raw material to support the production of plant meat in the future. Therefore, this study developed a 3D printable ink by mixing SPI with κC and alginate polysaccharides. The structural and functional properties of the ink were evaluated using rheology, texture analysis, Fourier transform infrared spectroscopy, and scanning electron microscopy. The study investigated the

interactions between protein and polysaccharides and their effects on the printability of the ink.

2. Materials and methods

2.1. Materials

SPI (protein content > 90%) was purchased from Shanghai yuanye Bio-Technology Co., Ltd (Shanghai, China). The ionic content of SPI was determined by atomic absorption spectrometry, and its composition was 0.02±0.01 wt% of Ca^{2+}, 0.04±0.00 wt% of K^{+} and 0.03±0.01 wt% of Na^{+}. Kappa-carrageenan (κC) and β-mercaptoethanol were acquired from Shanghai Aladdin Ltd (Shanghai, China). The ionic content of κC was determined by the same procedure, the contents were 3.5±0.05 wt% of K^{+}, 1.25±0.01 wt% of Na^{+}, 0.47±0.04 wt% of Ca^{2+}, 2.1±0.02 wt% of Cu^{2+}, and 3.2±0.03 wt% of Zn^{2+}. Sodium alginate (SA), tris (hydroxymethyl)methyl aminomethane (Tris), glycine, urea, sodium dodecyl sulfate (SDS), and disodium ethylenediaminetetraacetic acid (Na_2EDTA) were supplied by Shanghai Macklin Biochemical Technology Co., Ltd (Shanghai, China). The ionic content of SA was determined by the same procedure, the contents were 2.31±0.01 wt% of K^{+}, 11.23±0.02 wt% of Na^{+}, 0.03±0.01 wt% of Fe^{2+}. Bovine serum albumin (BSA) was obtained from Solarbio Science & Technology Co., Ltd (Beijing, China). All other reagents and chemicals were of analytical grade.

2.2. Food 3D Printing Ink Preparation

The mixtures of SPI with sodium alginate and κC were prepared as followed. SA and κC solutions were dissolved in deionized water at three concentrations (1, 1.5, and 2% w/w). Subsequently, mixed the two solutions and added SPI powder to the mixed solution to achieve a concentration of 15% (w/w) of SPI. Table 1 presents eight representative ink formulations with a gradient cross rise in two kinds of polysaccharides, the original ratio of SPI and polysaccharide was chosen according to Hu et al., (2017). The resulting mixed solution was homogenized using a homogenizer (HFJ-25, Hengao, Tianjin, China) at 500 rpm for 5 min until a stable suspension was formed. All samples had pH values within 6.8±0.3, which were above the isoelectric point of soy proteins (Lu et al., 2023). The resulting paste-like mixture was kept in a

water bath at 80 °C for 30 min and cooled at room temperature for 15 min. The samples were stored overnight in the refrigerator and heated to 25 °C before 3D printing.

2.3. 3D printing process

The samples were printed using an extrusion-based food 3D printer (FOODBOT-S2, Hangzhou Shiyin Technology Co., Ltd., Hangzhou, China). The prepared ink filled into the 3D printing nozzle syringe, and the printer extruded the material by controlling the movement of the plunger in accordance with the preset 3D mesh model (18.6 mm × 18.6 mm × 8 mm). The main printing parameters were set as follows: nozzle diameter of 0.84 mm, nozzle printing rate of 25 mm/s, layer height of 0.8 mm, printing temperature of 25 °C, extruded rate of 24 mm^3/s and infill density of 100% printing. To ensure maximum aseptic operation, all containers, nozzle syringes, and nozzle tips were sterilized at 121 °C in an autoclave for 15 min. The printing environment was disinfected with 75% ethanol and UV radiation, and all operations were conducted in a laminar flow hood.

2.4. Rheological Properties of Printing Inks

The rheological properties of the printing inks were measured using a hybrid rheometer (Discovery HR-2, DHR, TA Instruments, New Castle, DE, USA). A parallel plate with a diameter of 40 mm was used, with a measurement gap of 1 mm. When loading the sample, any excess material on the edges was removed with a scraper, and a thin layer of silicone oil was applied to the edges to prevent moisture evaporation. The configuration was set as follow: soak time was 180 s, 7 points were detected per decade, the interval between the points was 10 s, and the steady state sensing in DHR rheometer was applied to make sure the equilibrium time was 30 s for each point.

2.4.1. Flow sweep test

The flow sweep test was measured at shear rates ranging from 0.01 to 100 s^{-1}, with a temperature set at 25 °C, to obtain the viscosity η as a function of shear rate and investigate the shear-thinning behavior of the sample.

2.4.2. Amplitude sweep test

The linear viscoelastic region (LVR) was determined through an amplitude sweep test. The test was conducted within a strain range of 0.01-100% at a constant frequency

of 10 rad/s, and the experiment was performed at a temperature of 25 °C.

2.4.3. Frequency sweep test

The dynamic viscoelastic properties of the sample were evaluated through a frequency sweep test. The oscillation was performed within a frequency range of 0.1-100 rad/s, with a constant strain of 0.5% (within the LVR), and the experiment was conducted at a temperature of 25 °C. The storage modulus (G') loss modulus (G") and loss tangent (tan $\delta = G''/G'$) were recorded. All tests were repeated in triplicates, and experimental curves were plotted accordingly.

2.5. Texture analysis

Texture characteristics of the 3D printed samples were measured using a texture analyzer (TA. XT Plus, Stable Micro Systems, UK) equipped with a P36/R probe. The samples were tested as 18.6 × 18.6 × 8 mm grid-like architectures printed products for two compression cycles. The testing parameters were set as follows: the pre-test, test, and post-test speeds were all set at 1 mm/s, the trigger force was 10 g, the compression ratio was 50%, the time interval between the two compressions was 5 s, and the measurement temperature was 25 °C. Each sample was tested three times for repeatability.

2.6. Field-emission Scanning electron microscopy (FE-SEM) analysis

The microstructure of the paste was observed using a scanning electron microscope. The paste samples were freeze-dried, and the surface of the samples was sputter-coated with gold under vacuum conditions. The samples were then observed under the field-emission scanning electron microscope (S-4700, HITACHI, Japan) at different magnifications (1000×, 2500× and 5000×) with an accelerating voltage of 15 kV.

2.7. Molecular interaction analysis

To elucidate the paste cross-linking mechanism resulting from SPI-polysaccharide interactions, the protein solubility of the composite paste in five different solvents was measured to assess the intermolecular forces within the paste according to the method described by Wang et al. (2018). The paste sample (protein concentration 2 mg/mL) was dissolved in different solvents. The solvent S1 was distilled water, the solvent S2 consisted of 0.086 M Tris-0.09 M Glycine-4 mM-Na_2EDTA (pH = 8.0), the solvent S3

198 was 0.5% SDS, the solvent S4 was 8 M Urea, and solvent S5 was 2% β-
199 mercaptoethanol. The mixture samples (2.00 ± 0.02 g) were mixed with 10 mL buffer,
200 the resulting solution was incubated in a water bath at 25 °C for 20 min, and then
201 centrifuged at 5000 rpm for 10 min. The protein supernatant was determined using
202 bovine serum albumin as standard with ultraviolet spectrophotometry at 595 nm
203 (GENESYS 150, Thermo Fisher Scientific Inc, Waltham, MA, USA). The protein
204 solubility is expressed as the percentage of protein content of the supernatant in the
205 total protein content.

206 Tris-glycine buffer disrupts electrostatic interactions, SDS disrupts hydrophobic
207 interactions by disrupting the medium between the hydrophobic and hydrophilic
208 regions, urea disrupts hydrogen bonding in the protein by dehydrating the protein
209 molecules' side chains and backbone, and β-mercaptoethanol reduces protein disulfide
210 bonds by competing with thiol groups (Qin et al., 2017; Wang et al., 2021). According
211 to this method, the differences in protein solubility in S2 (Tris-Gly buffer)-S1 (distilled
212 water), S3 (0.5% SDS)-S2, S4 (urea)-S3, and S5 (β-mercaptoethanol)-S4 were used as
213 indications of the electrostatic interactions, hydrophobic interactions, hydrogen
214 bonding interactions, and disulfide bonding interactions, respectively.

215 **2.8. Fourier transform infrared spectroscopy (FTIR)**

216 The samples were mixed with dry KBr at a ratio of 1:100 (w/w). Then the mixed
217 powder was ground in the quartz mortar and pressed into a tablet. FTIR spectra (Nicolet
218 6700, Thermo Fisher Scientific Inc, USA) was performed at 25 °C in the range of 4000
219 to 500 cm^{-1}. The resolution remains at 1 cm^{-1}.

220 **2.9. X-ray diffraction (XRD)**

221 The X-ray diffraction (XRD) patterns of Cu Kα radiation (λ = 0.1541 nm) were
222 recorded by powder diffractometer (Empyrean, Malvern PANalytical, NL). The
223 working voltage was 40 kV and the working current was 40 mA. The patterns were
224 collected with a 2θ range from 5° to 60° at a step of 0.0262°.

225 **2.10. Differential scanning calorimetry (DSC)**

226 Differential scanning calorimeter (DSC 8000, PE Instruments Inc., USA) was used
227 to evaluate the thermal properties of the composite pastes. The thermal analysis was
228 conducted according to the method described by Wang et al. (2018) with slight

modifications. Briefly, the sample mixture (10 mg) was accurately weighed and loaded into a DSC pan. Prior to analysis, the DSC pan was sealed and maintained at the initial scanning temperature of 20 °C. The sample was analyzed from 20 °C to 180 °C at a scanning rate of 10 °C/min, and the temperature of each endothermic or exothermic peak was determined. A sealed empty pan was used as a blank reference.

2.11. Statistical Analysis

The results are shown as the mean ± standard deviation (SD) of triplicate experiments. SPSS software (SPSS26; IBM SPSS Statistics, Chicago, IL, USA) was used for one-way ANOVA and Duncan tests at 95% confidence level for data analysis. All graphs in the experiment were drawn using Origin software (2020b, OriginLab, MA, USA).

3. Results and discussion

3.1. Printability of composite inks

Soy protein isolate (SPI), as the main material for printing, cannot be directly printed due to its high flowability and relatively weak cross-linking in water (Shi et al., 2023). Sodium alginate (SA) is a commonly used hydrophilic colloid with good binding capacity for proteins (Chen et al., 2022). Kappa-carrageenan (κC) is a soluble polysaccharide with high solubility and gelation properties (Bi et al., 2018). The addition of SA and κC to the SPI paste could improve the stability and printability of food ink. In order to screen ink formulations with optimal printing performance, this study prepared inks with different polysaccharide concentration ratios and examined their printability. The 3D printing results of different ink formulations are shown in Figure 1. The successful implementation of food 3D printing requires two conditions: the material in the extrusion process has the right viscosity to flow through the nozzle and adhere layer by layer, and the paste structure after extrusion has sufficient mechanical strength to ensure its formability (Osi et al., 2021). For preliminary tests of printability, the ink should be continuously extruded from the nozzle as a uniform filament, and the printed product should show the effect of perfect detail, smooth surface, and structural stability, rather than being unable to form or causing blockages and tangled (Figure 1).

In the blue irregular region, SPI paste collapsed immediately after continuous and uniform extrusion from the nozzle, showing the characteristics of some liquid-like fluids, and the 3D printing molding effect was poor, unable to form and support the designed three-dimensional grid structure. This could be due to the insufficient gelation capacity and the low viscosity, and the ink forms irregular printing filaments at the nozzle, resulting in the inability to form a homogeneous structure (Jiang et al., 2019). In the orange region, the ink formulation aggregates significantly at the nozzle when subjected to stress, which may be due to the inappropriate surface tension of the ink, leading to a tendency for rapid recovery and aggregation of the system after extrusion (Fu et al., 2021). In the gray region, as the polysaccharide content in the ink gradually increased, the viscosity of the sample increased, resulting in poor flowability of the ink material and the nozzle clogging (Fu et al., 2021). In the green printable region, ink components were able to be continuously and smoothly extruded. The ink can be printed when the concentration of SA changed from 1 wt% to 2.5 wt% with a κC concentration of 1 wt%, or when the concentration of SA changed from 1 wt% to 2.5 wt% with a κC concentration of 1.5 wt%. However, some ink formulations, such as S15A1K1.5, S15A1K1, and S15A1.5K1.5, print three-dimensional mesh structure filaments that are uneven and have broken structures. In contrast, the 3D mesh structures printed by the SPI15A1.5K1 and S15A2K1.5 formulations had good self-supporting properties, smooth surfaces and showed uniform layer thickness. Therefore, to investigate the reasons for the differences in printability among the different formulations and the effects of different polysaccharide concentrations on ink printability, five representative ink formulations (irregular: SPI 15; tangled: S15A2K2; clogged: S15A1.5K2; printable: S15A1.5K1.5 and S15A2K1.5) were selected for in-depth study.

3.2. Rheological properties

The rheological properties of the inks directly influence their printability for 3D printing based on extrusion samples, with viscosity being a key indicator of extrusion capability. As the polysaccharide concentration increased, the viscosity of the paste also increased. As shown in Figure 2a, all samples exhibited a shear rate-dependent

reduction in viscosity, demonstrating typical shear-thinning behavior, which is generally favorable for extrusion-based 3D printing (Dankar et al., 2018). This may be attributed to the disruption of polymer entanglement during the shear process, causing polymer chains to stretch and align parallel to the shear direction (Hou et al., 2022; Zhang et al., 2022). The stress and shear rate applied to the fluid during extrusion depends on the fluid and extrusion conditions, and these conditions can vary greatly in different applications (Lopez Hernandez et al., 2021). The apparent shear rate of a steady-state pipe can be derived by extruding the corresponding flow rate and tube radius (Xie et al., 2020).

$$\dot{\gamma} = \frac{3.34Q}{\pi R^3}$$

Where Q is the volumetric flow rate and R is the tube inner radius. According to the volumetric flow (24 mm^3/s) and inner radius (0.42 mm), the calculated shear rate is about 344.4 s^{-1}. This result is fitted with the report of (Lopez Hernandez et al., 2021). The viscosity of the SPI 15 ink at the high shear rate (100 s^{-1}) is much lower than the viscosity at the low shear rate of 0.1 s^{-1}. This is because at very low shear rates, the stable aggregates formed by the glycine subunits of SPI are stabilized by disulfide bonds, and the side chains are entangled with adjacent chains, resulting in high viscosity. As the shear rate increases, the unraveling of the side chains and the arrangement of the molecules provide less shear resistance, thereby reducing the viscosity (Dorishetty et al., 2019). Some studies have added *Lycium barbarum* polysaccharide to soy protein isolate, and the results show that the apparent viscosity increases significantly with the addition of polysaccharide in a concentration-dependent manner (Xing et al., 2024). In our experiment, the slope of the viscosity versus shear rate was not smooth, which is also observed in other studies (Lu et al., 2023, Liu et al., 2022, Yu et al.,2022 and Chen et al., 2019). This may be because the sample has not yet reached equilibrium, especially at a high shear rate. In the high shear rate region (i.e. from 1 to 100·s^{-1}), molecules or particles within the fluid may not have enough time to rearrange and adjust their positions. Besides, it is speculated that the turbulent flow happened or the sample slipped out at the higher shear rate. At the shear rate of 1 s^{-1}, the viscosity of S15A1.5K2,

S15A1.5K1.5, and SPI 15 food inks was 1.22×10^3 Pa s, 9.81×10^2 Pa s and 9.06×10^2 Pa s, respectively. The viscosity range of S15A1.5K1.5 ink is similar to the results of (Dick et al., 2020). Among them, the viscosity of more than 1200 Pa s will lead to entanglement of ink molecules, insufficient pressure in the cylinder, resulting in nozzle clogging. If the viscosity was less than 900 Pa s, although it is easy to squeeze, the fluidity was too large to provide sufficient viscoelasticity and stability. Therefore, an ideal viscosity for the ink should be known during the extrusion process, which allows the ink to pass through the narrow diameter of the printing nozzle while maintaining its deposition structure and shape.

The nonlinear rheological behavior of samples can be monitored by large amplitude oscillatory shear test. The linear viscoelastic range (LVER) and critical strain of ink formulations with different compositions are shown in Figure 2b. LVER is a range where the storage modulus G' and loss modulus G" remain relatively constant as shear intensity increases. The G' is a measure of the elastic solid-like behavior, that is, the resistance to elastic deformation of the sample, while the G" is the viscous response, which is the ratio of stress to strain under vibration conditions (Yang et al., 2018). When G' is greater than G", the material behaves primarily as a solid, and vice versa for a viscous fluid, exhibited a slight frequency dependence (Pan et al., 2022). Within this range, the material undergoes elastic deformation and can recover to its original state after the stress is removed. As shown in Figure 2b, when the applied strain is less than 1%, different inks have similar LVERs, maintaining stable values. As the strain increased, the value of G' started to decrease, indicating the critical point of the elastic properties of the samples about 1-2%. The weak gelation ability of SPI at room temperature results in disordered polymer chains and poor stability, leading to a liquid-like state after extrusion (Fu et al., 2021). There is a clear positive correlation between G' and the polysaccharide concentration in the ink, where G' increases sequentially for inks S15A1.5K1.5 and S15A2K1.5, indicating higher structural strength, which aligns with the results of viscosity tests. Among them, ink S15A1.5K1.5 showed the lowest G' value in all the ink formulations with added polysaccharides. This may be due to a low polysaccharide concentration, which prevents the ink system from forming a stable

paste structure.

Frequency sweep tests can provide information about the internal structure of the printing inks (Hou et al., 2022). As shown in Figure 2c and, 2d, the G' and G" of all pastes exhibit a steady upward trend, with G' being superior to G", indicating that the ink primarily possesses elastic and solid characteristics. Higher polysaccharide content in the paste could leads to higher cross-linking density in the SPI-polysaccharide system, resulting in stronger viscoelasticity and mechanical strength of the paste, as well as good self-supporting properties and resistance to shape deformation (Pan et al., 2022). This might be attributed to the formation of a denser and more robust intermolecular cross-linking structure through molecular interactions between polysaccharides and SPI, exhibiting stronger solid characteristics. The loss tangent, tan δ = G"/G', is used as a characteristic parameter to account for the different viscoelastic behaviors. A tan δ value less than 1 indicates a predominantly elastic property, while a tan δ value greater than 1 indicates a predominantly viscous property (Yang et al., 2018). The tan δ values of all samples were less than 1, which indicated that the addition of polysaccharide enhanced the gel properties of the mixture and made it form a rigid gel structure. The addition of κC can induce electrostatic interactions with proteins, leading to the predominant solid-like behavior of these fluids (Lu et al., 2022). Among them, with a constant κC concentration of 1.5 wt% and angular frequency of 10 rad/s, when the SA concentration was increased from 1.5 wt% to 2 wt%, G' and G" increase from 24970.3 Pa and 4042.66 Pa to 30697.3 Pa and 4845.1 Pa, respectively. G' increased by 22.94% and G" increased by 19.85%. However, with a constant SA concentration of 2 wt% and angular frequency of 10 rad/s, when the κC concentration was increased from 1.5 wt% to 2 wt%, G' and G" increased from 30697.3 Pa and 4845.1 Pa to 32279.5 Pa and 5002.04 Pa, respectively. G' increased by 51.54% and G" increased by 3.24%. These results suggest that polysaccharides participate in the formation of the paste structure, and different types of polysaccharides lead to different structures. It has been reported that with the increase of κC concentration, the interaction between κC-proteins may gradually decrease and be replaced by the κC-κC interaction (Lu et al., 2022). Some studies have shown that the gel strength of calcium alginate gels is relatively weak (Fernández Farrés

et al., 2013). Compared to SA, κC has a greater impact on the viscoelasticity of the paste, and at higher concentrations, the paste structure becomes more rigid. However, excessively high viscoelasticity of the paste may have adverse effects on 3D printing, as the generated high shear forces can hinder ink extrusion or cause fracture after extrusion. On the other hand, the higher the concentration of SA, the smoother the extrusion process, the flatter the filaments, making it more suitable for printing, which will be confirmed by the results of texture analysis.

In general, the printability of soybean protein-polysaccharide composite paste is aimed at printing out self-supporting, flat sample and smooth surface. To ensure printability, the ink should exhibit contrasting properties. Initially, it must be fluid enough to be pumped and extruded, yet it should also stiffen rapidly after deposition to enable construction. Therefore, the amount of different polysaccharides added is particularly important, and the range of proper mechanical properties should be between 900 Pa s and 1200 Pa s.

3.3. Texture profile analysis (TPA)

Texture profile analysis can detect several texture parameters, including hardness, springiness, adhesiveness, and others (Yuan et al., 2016). As shown in Table 2, paste samples without polysaccharides cannot determine the TPA parameters due to their extremely weak gel properties, highlighting the importance of incorporating polysaccharides in the ink for the production of self-supporting 3D printed food products. With an increase in polysaccharide concentration, the springiness, cohesiveness, gumminess, and resilience of the printed samples all significantly decreased (Table 2). This could be attributed to the changes in the repulsive forces between polysaccharide charges that affect molecular aggregation. Both carrageenan and sodium alginate are anionic polysaccharides that can form complexes with the amino group ($-NH_3^+$) of the protein through electrostatic interactions, thereby altering the printing characteristics of the paste (Huang et al., 2021). Sulfated polysaccharides such as carrageenan have the ability to interact with proteins above their isoelectric point. κC contains a sulfate group ($-OSO_3^-$) that can be bonded to the amino group ($-NH_3^+$) of the protein by electrostatic interaction. The electrostatic interaction between

sulfate group (- OSO_3^-) and protein is stronger than that between carboxyl group (-COO-) and protein (Huang et al., 2021). Furthermore, SPI possesses a globular structure, and the folded SPI structure can stretch and expose internal functional group structures upon heating, facilitating cross-linking with polysaccharide ions.

Hardness refers to the force required to compress a sample and can mimic the chewing behavior of the oral cavity on solids or semi-solids, serving as an indicator of the structural stability of 3D printed food. Compared to pastes with the same concentration of SA, the addition of κC significantly affects the properties, with an increase in sample hardness and a decrease in adhesiveness and springiness. When the κC concentration reached 2 wt%, high shear forces occur during the extrusion process, leading to filament breakage at the nozzle, resulting in poor shape fidelity and significant discrepancies between the printed samples and the intended model, making it also impossible to determine the TPA parameters. In contrast, the addition of SA, with the same concentration of κC, yields opposite results. This may be attributed to the disruption of the molecular chain structure of the samples during preparation, where longer polysaccharide chains exhibit stronger gelation properties with proteins (Monteiro & Lopes-da-Silva, 2017). The springiness of the samples refers to the physical reboundness after deformation, which can resist to external forces. At higher concentrations, polysaccharides dominate the springiness of the mixture, leading to a weakening of samples structure, as also reflected in the aforementioned rheological analysis (Warnakulasuriya & Nickerson, 2018). This is contrary to the experimental conclusion of (Xu et al.,2023). This result may be due to the fact that the sample has a hollow structure, and when the extrusion degree is 50%, the sample is forced to extrude from all sides to widen, resulting in a decrease in data presentation. Cohesiveness refers to the adhesive forces within the sample particles, reflecting the magnitude of intermolecular binding forces that allow the sample to maintain its integrity even under pressure. The data indicates that there is only a minor difference in cohesiveness between the samples, and the low concentration of polysaccharide improved the structural properties of the paste. When the concentration of polysaccharide was too high (>1.5%, wt %), the Cohesiveness and resilience of the sample decreased, which

was consistent with the results of (Xu et al.,2023). This may be attributed to changes in the repulsive forces between the negative charges in the polysaccharide, which affect molecular aggregation and thus alter the texture properties of the sample (Xu et al.,2023). The above results suggested a positive correlation between paste textural properties and polysaccharide concentration. Considering that plant-based foods are extruded with current inks as the main material, the protein paste having the formulations S15A1.5K1.5 exhibits optimal texture properties and is most suitable for 3D printing. In fact, the texture of plant-based foods largely depends on their structure, mechanical properties, and surface characteristics (Shi et al., 2023).

3.4. Microstructure

Figure 3 illustrates the microstructures of different ink formulations at various magnifications (1000×, 2500×, and 5000×). All food inks exhibit a heterogeneous microstructure composed of protein-polysaccharide particles forming aggregates. The structure of soybean isolate protein (SPI) has a rough surface because it is a paste at room temperature. However, the structural support provided by these concentrations is still insufficient to meet the required criteria, which may be the reason for the inability to achieve proper printability (Figure 1). Therefore, an appropriate polysaccharide concentration needs to be added to achieve gelation. Different ink formulations have different densification and orientation of the cavity, which is especially obvious after the addition of polysaccharides. Sodium alginate (SA) and kappa carrageenan (κC) bind strongly to protein particles, forming small fragmented block formations. SA, κC, and SPI particles form non-covalent bonds due to their hydrophilic nature and abundance of carboxyl and hydroxyl groups, which promote hydrophobic interactions and hydrogen bonding (Huang et al., 2021; Wei et al., 2023). As the κC content increased, the cross-linking structure with SPI-polysaccharide particles became rougher, resulting in a more disordered and chaotic ink system, forming large aggregates. This could be an increased interaction between κC and κC (Lu et al., 2022). This may explain why ink S15A1.5K1.5 was able to be extruded from the nozzle while ink S15A1.5K2 became clogged and ink S15A2K2 agglomerated (Figure 1). SA more ink formula surface is more compact and smoother, which is consistent with (Chen et al., 2022).

Overall, ink S15A1.5K1.5 has the best network density and can resist structural changes under high shear stress during the extrusion process.

3.5. Molecular interaction force analysis

As shown in Figure 4a, the solubility of the composite paste was significantly enhanced, indicating the presence of hydrophobic interactions, electrostatic interactions, disulfide bonds, and hydrogen bonds within the protein paste structure. The interaction forces between protein molecules and polysaccharides followed the order of hydrophobic interactions > electrostatic interactions > disulfide bond interactions > hydrogen bond interactions. This observation was consistent with the previously reported results (Lu et al., 2023). A slight decrease in electrostatic interactions was observed in the composite paste. This result can be attributed to the influence of negatively charged groups on the protein and polysaccharide surfaces, which are affected by the electrostatic binding under high polysaccharide concentrations, leading to conformational changes in the protein and exposing more hydrophobic groups (Wang et al., 2021). When electrostatic repulsion further increases, the distance between molecules becomes longer, making it difficult to detect the signal of electrostatic repulsion, resulting in decreased solubility. Compared to pure SPI paste, the addition of polysaccharides significantly increased hydrophobic interactions and hydrogen bond interactions in the paste ($p < 0.05$). This finding indicates that the addition of polysaccharides greatly enhances hydrophobic interactions and hydrogen bond interactions, playing a crucial role in the formation and maintenance of the SPI-polysaccharide paste system. This phenomenon may be attributed to the exposure of chemical groups within the protein matrix after thermal treatment. SA and κC are anionic acidic polysaccharides rich in carboxyl and hydroxyl groups. Although there is an intrinsic repulsion between them, but other forces can maintain the state without causing the system to separate, especially at high concentrations. Studies have shown that there is an electrostatic interaction between SPI and κC, where the negatively charged sulfate groups on κC can interact with the positively charged amino groups (-$OSO_3^-NH_3^+$) on proteins, even at pH above the isoelectric point (Huang et al., 2021; Lu et al., 2023). Additionally, SPI and polysaccharides can absorb moisture, promoting

498 further aggregation of proteins and overcoming the biocompatibility and inherent
499 repulsion between SPI and polysaccharides, ultimately forming a paste cross-linking
500 structure (Cao et al., 2022; Min et al., 2022).

501 **3.6. Composite paste forming mechanism**

502 Based on the intermolecular interactions and rheological properties discussed
503 above, this study presents a plausible hypothesis regarding the gelation mechanism of
504 SPI-polysaccharide (Figure 5). The experimental results revealed that hydrophobic
505 interactions and electrostatic interactions are the predominant forces in the composite
506 paste. Heating facilitates the exposure of hydrophobic groups in the protein, while the
507 polysaccharides SA and κC contain numerous carboxyl and hydroxyl groups,
508 enhancing hydrophobic interactions and hydrogen bonding with SPI particles (Huang
509 et al., 2021; Wei et al., 2023). The presence of a substantial number of hydrophobic
510 groups leads to protein crosslinking and aggregation. κC, on average, contains an
511 anionic sulfate group (- OSO_3^-) per disaccharide repeating unit, which can engage in
512 electrostatic interactions with cationic groups (-NH_3^+) of the protein. The electrostatic
513 interaction between sulfate group (- OSO_3^-) and protein is stronger than that between
514 carboxyl group (-COO-) and protein (Huang et al., 2021; Lu et al., 2023). In the SPI
515 system, the addition of κC forms protein-polysaccharide interactions, establishing a
516 balance between protein-protein and protein-polysaccharide interactions. This is
517 consistent with the fact that in all oscillation studies, the composite gel is visually
518 homogeneous and there is no phase separation. When the polysaccharide concentration
519 exceeds 1.5 wt%, the self-aggregation of polysaccharides hinders SPI cross-linking,
520 reducing its interaction with SPI. As the κC content increases, the κC -κC interaction
521 increases and the κC -protein interaction decreases, resulting in a stronger gel that is
522 unable to extrude from the nozzle. The molecular structure of SA is rich in hydroxyl
523 and carboxylic groups, and it is easy to form intermolecular hydrogen bonds with the
524 functional groups of other polymers (Wei et al., 2023). However, it has been reported
525 that SA alone exhibits inadequate mechanical properties in soft tissue engineering
526 applications, failing to provide sufficient mechanical support under stress conditions,
527 which aligns with our experimental results (Wei et al., 2023). But when the addition

amount of SA exceeds a certain critical value (2.5 wt%), it forms a gel with soybean protein, yielding improved printing performance. Some studies have successfully prepared alginate/carrageenan composite hydrogels with different concentrations of carrageenan, and bio-printed the alginate/carrageenan scaffold, the results show that the gel is suitable for using bioprinting to manufacture 3D hydrogel scaffold (Kim et al., 2019).

3.7. Fourier transform infrared (FTIR) analysis

In order to investigate the changes in chemical bonds in the inks, a comparison of their FTIR spectra was conducted, as shown in Figure 4b. The FTIR spectra of the paste samples did not exhibit any new peaks upon the addition of polysaccharides, and there were no new functional groups observed with varying ratios of SA and κC, indicating that the covalent interactions were minor. This is consistent with the research results of (Xing et al., 2024). All inks displayed a strong and broad absorption peak in the range of 3200-3600 cm^{-1}, which is typically associated with the stretching of O-H bonds and partially formed hydrogen bonds (Yu et al., 2022). Compared to the SPI 15, the O-H stretching bands of the ink with added polysaccharides shifted to lower wavenumbers. For instance, in the inks S15A2K1.5 and S15A2K2, the band of the SPI 15 ink at 3273 cm^{-1} shifted to 3282 cm^{-1} and 3286 cm^{-1}, respectively, suggesting stronger hydrogen bonding and increased molecular interactions in the S15A2K2 ink (Min et al., 2022). In fact, hydrogen bonding can form connections between proteins and polysaccharides, enhancing cross-linking strength, which is crucial for controlling the printability of different biomacromolecules in food inks (Warnakulasuriya & Nickerson, 2018). In all mixed pastes, weak peaks were also observed in the range of 2998-3018 cm^{-1}, which could be attributed to the stretching vibrations of C-H bonds (Min et al., 2022). Furthermore, all inks exhibited a peak at approximately 1633 cm^{-1}, which is related to the asymmetric and symmetric stretching of carboxylate groups (COO-) and has been suggested to be caused by the bending vibrations of water molecules (1650 cm^{-1}) (Hu et al., 2017; Shi et al., 2023). It is noteworthy that when different polysaccharides were added to SPI, all inks showed absorption peaks in the range of 1515-1531 cm^{-1}, with the bands shifting from higher to lower wavenumbers. These peaks are associated with

the amide I (1600–1700 cm^{-1}) and amide II (1500–1600 cm^{-1}) regions in the FT-IR spectra. The amide regions primarily represent the stretching vibrations of C=O, the bending vibrations of N-H, and the stretching vibrations of C-N, which are reliable indicators of protein secondary structure conformation (Carbonaro & Nucara, 2010). The shift of bands from higher to lower wavenumbers indicates a decrease in the content of α-helical structures and an increase in the proportion of β-sheet structures in the paste (Liu et al., 2022). The results demonstrate that the combination of polysaccharides and SPI significantly alters the spatial structure of the paste.

3.8. X-ray diffraction (XRD) analysis

The X-ray diffraction patterns can be used to determine the amorphous or crystalline nature of molecules (Dong et al., 2021). As shown in Figure 4c, SPI exhibits two sharp peaks at diffraction angles of 9° and 19°, indicating its crystalline structure. Its primary structure is believed to consist of an α-helical and β-sheet structure (Chen et al., 2013; Dong et al., 2021). In contrast, the addition of polysaccharides to the composite paste results in two relatively flat peaks around 9°, suggesting a significant reduction in the α-helical structure and a presumed transition to the β-sheet structure. This also indicates the formation of amorphous complexes between SPI and polysaccharide molecules. Such amorphous nature is directly related to the hydrophilicity and hygroscopicity of the polymer (Wang et al., 2018). Composite pastes prepared with formulations S15A1.5K1.5 and S15A1.5K2 exhibit broad diffraction peaks at approximately 19°, while formulations S15A2K1.5 and S15A2K2 show increased peak intensities and sharpened peaks. These structural changes suggested a corresponding interplay between the α-helical and β-sheet structures, with an increase in SA concentration potentially leading to the transformation of the α-helical structure to the β-sheet structure in the paste samples (Pan et al., 2022). It has been found that β-sheet structures have greater potential energy compared to α-helices, which can explain why the composite paste exhibits a more stable structure than the SPI paste (Ding et al., 2003). When the SA concentration is 1.5 wt%, the peak intensity of the composite paste significantly weakens. This indicates good compatibility between the two polymers (Y. Dong et al., 2021). At an SA concentration of 2 wt%, the peak intensity increases and

becomes sharper around 19°, indicating the formation of amorphous complexes and intermolecular interactions. These results demonstrated that the presence of κC and SA influences the crystallinity of the SPI paste system making it promising for 3D printing.

3.9. Differential scanning calorimetry (DSC) analysis

The properties and structure of most substances vary with temperature, and therefore, the stability of the sample structure can be reflected by the changes in endothermic and exothermic behavior in the DSC spectra. The enthalpy change and transition temperature can be determined based on the temperature and peak area corresponding to the largest peak in the graph (Hou et al., 2022). The influence of different polysaccharide concentrations on the thermal stability of the composite paste is shown in Figure 4d. The addition of the polysaccharides significantly affects the thermal transition temperature, resulting in an upward shift of the melting temperature from 89.6 °C to higher temperatures as the polysaccharide content increases. The melting temperatures for S15A1.5K1.5, S15A1.5K2, S15A2K1.5, and S15A2K2 are 95.3 °C, 92.8 °C, 93.5 °C, and 95.2 °C, respectively. This can be attributed to the interaction between the amino and carboxyl groups of SPI and the hydroxyl groups of the polysaccharides through hydrogen bonding, consistent with the aforementioned intermolecular forces. As the polysaccharide quantity increases, the melting temperature of the composite paste gradually rises, indicating a higher amount of heat absorbed during the sample melting process and an enhancement in thermal stability. Within the melting temperature range, SA and κC in the composite paste may form a cross-linked structure, with some SPI potentially participating in the formation of the structure and being encapsulated within it. This promotes the stability of the dense cross-linking system, ultimately leading to changes in thermal stability. These findings suggest a certain degree of interaction between SPI and polysaccharides, resulting in a covalently cross-linked composite paste system, which could explain the paste's elasticity, viscosity, and strength.

4. Conclusion

In this study, a 3D printable ink was prepared using soy protein isolate, carrageenan, and sodium alginate. The addition of polysaccharides to soy protein at

appropriate concentrations facilitated the interaction between proteins and polysaccharides, resulting in protein-polysaccharide pastes with optimal 3D printing quality. This combination provides a viable method for the production innovative of plant-based foods. Rheological and textural analyses revealed that the addition of polysaccharides increased the viscosity and hardness of the printing ink. The S15A1.5K1.5 ink exhibited favorable viscosity and storage modulus (G'), enabling stable printability. FT-IR analysis and molecular interaction within the dense cross-linking indicated that the introduction of polysaccharides led to the formation of hydrogen bonds through the -OH groups, transforming α-helices into β-sheets. Hydrophobic interactions, electrostatic interactions, and disulfide bonding were identified as the main driving forces maintaining the paste structure. SEM images displayed the rough surface of the composite material, confirming the formation of a dense cross-linking structure between SPI and polysaccharides. XRD results indicated that the interactions between SPI and polysaccharides led to a transition from a crystalline to an amorphous structure. DSC analysis demonstrated that the addition of polysaccharides significantly enhanced the thermal stability of the composite paste. These findings contribute to the improvement of texture and quality in protein-polysaccharide pastes, as well as the practical application of 3D printing technology in plant-based food, establishing both theoretical and practical foundations. In our next studies, we will explore various ink formulations using other types of food ingredients, such as pea protein isolate, to meet specific nutritional requirements of individuals.

Acknowledgements

This work was supported by the Key Research and Development Projects of Zhejiang [grant numbers 2022C04021, 2022C02041]; the Zhejiang Provincial Natural Science Foundation [grant number LQ23C200013].

References

Bi, C.-h., Zhu, Y.-d., Li, L.-t., Zhang, Y.-l., Hua, Z., Zhu, J.-y., Liu, Y., Liu, Y.-d., & Huang, Z.-g. (2018). Rheological properties and microstructure of soy protein isolate /κ-carrageenan gels under high-speed shear treatment. *Journal of Food Engineering*, *236*, 44-50. https://doi.org/10.1016/j.jfoodeng.2018.05.006

Cao, J., Tong, X., Wang, M., Tian, T., Yang, S., Sun, M., Lyu, B., Cao, X., Wang, H., & Jiang, L. (2022). Soy Protein Isolate/Sodium Alginate Microparticles under Different pH Conditions: Formation Mechanism and Physicochemical Properties. *Foods*, *11*(6), 790. https://doi.org/10.3390/foods11060790

Carbonaro, M., & Nucara, A. (2010). Secondary structure of food proteins by Fourier transform spectroscopy in the mid-infrared region. *Amino Acids*, *38*(3), 679-690. https://doi.org/10.1007/s00726-009-0274-3

Chen, Jingwang, Mu, T., Goffin, D., Blecker, C., Richard, G., Richel, A., & Haubruge, E. (2019). Application of soy protein isolate and hydrocolloids based mixtures as promising food material in 3D food printing. *Journal of Food Engineering*, *261*, 76-86. https://doi.org/10.1016/j.jfoodeng.2019.03.016

Chen, Jingwang, Sun, H., Mu, T., Blecker, C., Richel, A., Richard, G., Jacquet, N., Haubruge, E., & Goffin, D. (2022). Effect of temperature on rheological, structural, and textural properties of soy protein isolate pastes for 3D food printing. *Journal of Food Engineering*, *323*, 110917. https://doi.org/10.1016/j.jfoodeng.2021.110917

Chen, Jun, Chen, X., Zhu, Q., Chen, F., Zhao, X., & Ao, Q. (2013). Determination of the domain structure of the 7S and 11S globulins from soy proteins by XRD and FTIR. *Journal of the Science of Food and Agriculture*, *93*(7), 1687-1691. https://doi.org/10.1002/jsfa.5950

Cheng, Y., Fu, Y., Ma, L., Yap, P. L., Losic, D., Wang, H., & Zhang, Y. (2022). Rheology of edible food inks from 2D/3D/4D printing, and its role in future 5D/6D printing. *Food Hydrocolloids*, *132*, 107855. https://doi.org/10.1016/j.foodhyd.2022.107855

Dankar, I., Haddarah, A., Omar, F. E. L., Sepulcre, F., & Pujolà, M. (2018). 3D printing technology: The new era for food customization and elaboration. *Trends in Food Science & Technology*, *75*, 231-242. https://doi.org/10.1016/j.tifs.2018.03.018

Dick, A., Bhandari, B., Dong, X., & Prakash, S. (2020). Feasibility study of hydrocolloid incorporated 3D printed pork as dysphagia food. *Food Hydrocolloids*, *107*, 105940. https://doi.org/10.1016/j.foodhyd.2020.105940

Ding, F., Borreguero, J. M., Buldyrey, S. V., Stanley, H. E., & Dokholyan, N. V. (2003). Mechanism for the α-helix to β-hairpin transition. *Proteins: Structure, Function, and Bioinformatics*, *53*(2), 220-228. https://doi.org/10.1002/prot.10468

Dong, Die, & Cui, B. (2021). Fabrication, characterization and emulsifying properties of potato starch/soy protein complexes in acidic conditions. *Food Hydrocolloids*, *115*, 106600. https://doi.org/10.1016/j.foodhyd.2021.106600

Dong, Y., Huang, Z., Niu, L., & Xiao, J. (2021). Influence of kappa-carrageenan on the gel properties of auricularia auricular-judae during freeze–thaw cycles. *International Journal of Food Science & Technology*, *56*(2), 1048-1060. https://doi.org/10.1111/ijfs.14760

Dorishetty, P., Balu, R., Sreekumar, A., de Campo, L., Mata, J. P., Choudhury, N. R., & Dutta, N. K. (2019). Robust and Tunable Hybrid Hydrogels from Photo-Cross-Linked Soy Protein Isolate and Regenerated Silk Fibroin. *ACS Sustainable Chemistry & Engineering*, *7*(10), 9257-9271.

10.1021/acssuschemeng.9b00147

Fernández Farrés, I., Douaire, M., & Norton, I. T. (2013). Rheology and tribological properties of Ca-alginate fluid gels produced by diffusion-controlled method. *Food Hydrocolloids*, *32*(1), 115-122. https://doi.org/10.1016/j.foodhyd.2012.12.009

Fu, Z., Naghieh, S., Xu, C., Wang, C., Sun, W., & Chen, X. (2021). Printability in extrusion bioprinting. *Biofabrication*, *13*(3), 033001. https://doi.org/10.1088/1758-5090/abe7ab

Hou, Y., Liu, H., Zhu, D., Liu, J., Zhang, C., Li, C., & Han, J. (2022). Influence of Soybean Dietary Fiber on the properties of Konjac Glucomannan/κ-Carrageenan Corn Oil Composite Gel. *Food Hydrocolloids*, *129*, 107602. https://doi.org/10.1016/j.foodhyd.2022.107602

Hu, B., Chen, Q., Cai, Q., Fan, Y., Wilde, P. J., Rong, Z., & Zeng, X. (2017). Gelation of soybean protein and polysaccharides delays digestion. *Food Chemistry*, *221*, 1598-1605. https://doi.org/10.1016/j.foodchem.2016.10.132

Huang, M., Mao, Y., Li, H., & Yang, H. (2021). Kappa-carrageenan enhances the gelation and structural changes of egg yolk via electrostatic interactions with yolk protein. *Food Chemistry*, *360*, 129972. https://doi.org/10.1016/j.foodchem.2021.129972

Jiang, H., Zheng, L., Zou, Y., Tong, Z., Han, S., & Wang, S. (2019). 3D food printing: main components selection by considering rheological properties. *Critical reviews in food science and nutrition*, *59*(14), 2335-2347. https://doi.org/10.1080/10408398.2018.1514363

Keerthana, K., Anukiruthika, T., Moses, J. A., & Anandharamakrishnan, C. (2020). Development of fiber-enriched 3D printed snacks from alternative foods: A study on button mushroom. *Journal of Food Engineering*, *287*, 110116. https://doi.org/10.1016/j.jfoodeng.2020.110116

Kim, M. H., Lee, Y. W., Jung, W.-K., Oh, J., & Nam, S. Y. (2019). Enhanced rheological behaviors of alginate hydrogels with carrageenan for extrusion-based bioprinting. *Journal of the Mechanical Behavior of Biomedical Materials*, *98*, 187-194. https://doi.org/10.1016/j.jmbbm.2019.06.014

Liu, Z., Bhandari, B., Prakash, S., Mantihal, S., & Zhang, M. (2019). Linking rheology and printability of a multicomponent gel system of carrageenan-xanthan-starch in extrusion based additive manufacturing. *Food Hydrocolloids*, *87*, 413-424. https://doi.org/10.1016/j.foodhyd.2018.08.026

Liu, Z., Xing, X., Xu, D., Chitrakar, B., Hu, L., Hati, S., Mo, H., & Li, H. (2022). Correlating rheology with 3D printing performance based on thermo-responsive κ-carrageenan/Pleurotus ostreatus protein with regard to interaction mechanism. *Food Hydrocolloids*, *131*, 107813. https://doi.org/10.1016/j.foodhyd.2022.107813

Lopez Hernandez, H., Souza, J. W., & Appel, E. A. (2021). A Quantitative Description for Designing the Extrudability of Shear-Thinning Physical Hydrogels. *Macromolecular Bioscience*, *21*(2), 2000295. https://doi.org/10.1002/mabi.202000295

Lu, Z., Lee, P.-R., & Yang, H. (2022). Chickpea flour and soy protein isolate interacted with κ-carrageenan via electrostatic interactions to form egg omelets analogue. *Food Hydrocolloids*, *130*, 107691. https://doi.org/10.1016/j.foodhyd.2022.107691

Lu, Z., Lee, P.-R., & Yang, H. (2023). Kappa-carrageenan improves the gelation and structures of soy protein isolate through the formation of hydrogen bonding and electrostatic interactions. *Food Hydrocolloids*, *140*, 108585. https://doi.org/10.1016/j.foodhyd.2023.108585

Min, C., Ma, W., Kuang, J., Huang, J., & Xiong, Y. L. (2022). Textural properties, microstructure and digestibility of mungbean starch–flaxseed protein composite gels. *Food Hydrocolloids*, *126*, 107482. https://doi.org/10.1016/j.foodhyd.2022.107482

Monteiro, S. R., & Lopes-da-Silva, J. A. (2017). Effect of the molecular weight of a neutral polysaccharide on soy protein gelation. *Food Research International*, *102*, 14-24. https://doi.org/10.1016/j.foodres.2017.09.066

Osi, A. R., Zhang, H., Chen, J., Zhou, Y., Wang, R., Fu, J., Müller-Buschbaum, P., & Zhong, Q. (2021). Three-Dimensional-Printable Thermo/Photo-Cross-Linked Methacrylated Chitosan−Gelatin Hydrogel Composites for Tissue Engineering. *ACS Applied Materials & Interfaces*, *13*(19), 22902-22913. https://doi.org/10.1021/acsami.1c01321

Pan, H., Pei, F., Ma, G., Ma, N., Zhong, L., Zhao, L., & Hu, Q. (2022). 3D printing properties of Flammulina velutipes polysaccharide-soy protein complex hydrogels. *Journal of Food Engineering*, *334*, 111170. https://doi.org/10.1016/j.jfoodeng.2022.111170

Phuhongsung, P., Zhang, M., & Devahastin, S. (2020). Investigation on 3D printing ability of soybean protein isolate gels and correlations with their rheological and textural properties via LF-NMR spectroscopic characteristics. *Lwt*, *122*, 109019. https://doi.org/10.1016/j.lwt.2020.109019

Qin, X.-S., Chen, S.-S., Li, X.-J., Luo, S.-Z., Zhong, X.-Y., Jiang, S.-T., Zhao, Y.-Y., & Zheng, Z. (2017). Gelation Properties of Transglutaminase-Induced Soy Protein Isolate and Wheat Gluten Mixture with Ultrahigh Pressure Pretreatment. *Food and Bioprocess Technology*, *10*(5), 866-874. https://doi.org/10.1007/s11947-017-1864-9

Rowat, S. J. A., Legge, R. L., & Moresoli, C. (2021). Plant protein in material extrusion 3D printing: Formation, plasticization, prospects, and challenges. *Journal of Food Engineering*, *308*, 110623. https://doi.org/10.1016/j.jfoodeng.2021.110623

Shi, H., Li, J., Xu, E., Yang, H., Liu, D., & Yin, J. (2023). Microscale 3D printing of fish analogues using soy protein food ink. *Journal of Food Engineering*, *347*, 111436. https://doi.org/10.1016/j.jfoodeng.2023.111436

Wang, Wenjie, Shen, M., Jiang, L., Song, Q., Liu, S., & Xie, J. (2020). Influence of Mesona blumes polysaccharide on the gel properties and microstructure of acid-induced soy protein isolate gels. *Food Chemistry*, *313*, 126125. https://doi.org/10.1016/j.foodchem.2019.126125

Wang, Wenjie, Shen, M., Liu, S., Jiang, L., Song, Q., & Xie, J. (2018). Gel properties and interactions of Mesona blumes polysaccharide-soy protein isolates mixed gel: The effect of salt addition. *Carbohydrate Polymers*, *192*, 193-201. https://doi.org/10.1016/j.carbpol.2018.03.064

Wang, Ya-Ru, Yang, Q., Li-Sha, Y.-J., & Chen, H.-Q. (2021). Structural, gelation properties and microstructure of rice glutelin/sugar beet pectin composite gels: Effects of ionic strengths. *Food Chemistry*, *346*, 128956. https://doi.org/10.1016/j.foodchem.2020.128956

Warnakulasuriya, S. N., & Nickerson, M. T. (2018). Review on plant protein–polysaccharide complex coacervation, and the functionality and applicability of formed complexes. *Journal of the Science of Food and Agriculture*, *98*(15), 5559-5571. https://doi.org/10.1002/jsfa.9228

Warner, E. L., Norton, I. T., & Mills, T. B. (2019). Comparing the viscoelastic properties of gelatin and different concentrations of kappa-carrageenan mixtures for additive manufacturing applications. *Journal of Food Engineering*, *246*, 58-66. https://doi.org/10.1016/j.jfoodeng.2018.10.033

Wei, Q., Zhou, J., An, Y., Li, M., Zhang, J., & Yang, S. (2023). Modification, 3D printing process and application of sodium alginate based hydrogels in soft tissue engineering: A review. *International Journal of Biological Macromolecules*, *232*, 123450. https://doi.org/10.1016/j.ijbiomac.2023.123450

Xie, R., Mukherjee, S., Levi, A. E., Reynolds, V. G., Wang, H., Chabinyc, M. L., & Bates, C. M. (2020).

Room temperature 3D printing of super-soft and solvent-free elastomers. *Science Advances*, *6*(46), eabc6900. 10.1126/sciadv.abc6900

Xing, H., Liu, X., Hu, Y., Hu, K., & Chen, J. (2024). Effect of Lycium barbarum polysaccharides on heat-induced gelation of soy protein isolate. *Food Hydrocolloids*, *147*, 109323. https://doi.org/10.1016/j.foodhyd.2023.109323

Xu, K., Wu, C., Fan, G., Kou, X., Li, X., Li, T., Dou, J., & Zhou, Y. (2023). Rheological properties, gel properties and 3D printing performance of soy protein isolate gel inks added with different types of apricot polysaccharides. *International Journal of Biological Macromolecules*, *242*, 124624. https://doi.org/10.1016/j.ijbiomac.2023.124624

Yang, F., Zhang, M., Bhandari, B., & Liu, Y. (2018). Investigation on lemon juice gel as food material for 3D printing and optimization of printing parameters. *Lwt*, *87*, 67-76. https://doi.org/10.1016/j.lwt.2017.08.054

Yu, J., Wang, X.-y., Li, D., Wang, L.-j., & Wang, Y. (2022). Development of soy protein isolate emulsion gels as extrusion-based 3D food printing inks: Effect of polysaccharides incorporation. *Food Hydrocolloids*, *131*, 107824. https://doi.org/10.1016/j.foodhyd.2022.107824

Yuan, C., Du, L., Zhang, G., Jin, Z., & Liu, H. (2016). Influence of cyclodextrins on texture behavior and freeze-thaw stability of kappa-carrageenan gel. *Food Chemistry*, *210*, 600-605. https://doi.org/10.1016/j.foodchem.2016.05.014

Zhang, C., Wang, C.-S., Therriault, D., & Heuzey, M.-C. (2022). Development of aqueous protein/polysaccharide mixture-based inks for 3D printing towards food applications. *Food Hydrocolloids*, *131*, 107742. https://doi.org/10.1016/j.foodhyd.2022.107742

Table captions

Table 1. Composition of different 3D printing ink formulations (wt%).

Table 2. Texture profile analysis (TPA) indicators for different 3D printed pastes with different formulations.

804 **Table 1**. Composition of different 3D printing ink formulations (wt%).

Inks	Water/(ml)	SPI/(g)	SA/(g)	κC /(g)
SPI 15	85	15	-	-
S15A1K1	85	15	1.0	1.0
S15A1K1.5	85	15	1.0	1.5
S15A1.5K1	85	15	1.5	1.0
S15A1.5K1.5	85	15	1.5	1.5
S15A1.5K2	85	15	1.5	2.0
S15A2K1.5	85	15	2.0	1.5
S15A2K2	85	15	2.0	2.0

805 In the codes listed for formulation column, S15AmKn food ink means that SPI, SA, and κC
806 constitute 15 wt%, m wt% and n wt%, respectively.

807

Table 2. Texture profile analysis (TPA) indicators for different 3D printed pastes with different formulations.

Sample	Hardness (g)	Adhesiveness	Springiness	Cohesiveness	Gumminess	Chewiness	Resilience (g•sec)
SPI 15	-	-	-	-	-	-	-
S15A1K1	529.27±14.13 ^{a}	-7.22±3.31 ^{a}	0.78±0.02 ^{a}	0.42±0.03 ^{a}	223.55±19.90 ^{a}	173.18±13.32 ^{a}	0.17±0.01 ^{a}
S15A1K1.5	552.91±20.28 ^{a}	-23.60±2.73 ^{c}	0.46±0.02 ^{c}	0.37±0.01 ^{b}	205.01±2.26 ^{b}	94.93±4.41 ^{b}	0.11±0.01 ^{b}
S15A1.5K1	480.10±8.76 ^{b}	-14.14±3.39 ^{b}	0.59±0.02 ^{b}	0.36±0.01 ^{bc}	172.20±4.56 ^{c}	101.65±5.83 ^{b}	0.11±0.01 ^{b}
S15A1.5K1.5	538.73±12.16 ^{a}	-56.24±1.93 ^{e}	0.45±0.02 ^{c}	0.33±0.01 ^{c}	180.06±7.39 ^{c}	81.88±2.62 ^{c}	0.08±0.00 ^{d}
S15A1.5K2	-	-	-	-	-	-	-
S15A2K1.5	429.84±7.18 ^{c}	-43.74±3.38 ^{d}	0.45±0.01 ^{c}	0.35±0.00 ^{bc}	150.22±2.08 ^{d}	67.47±0.47 ^{d}	0.10±0.00 ^{c}
S15A2K2	-	-	-	-	-	-	-

Values were expressed as the mean ± standard deviation (n = 3). Different letters indicated significant differences ($p < 0.05$) between values in the same column. "-" means not shaped. S15AmKn food ink means that SPI, SA, and κC constitute 15 wt%, m wt% and n wt%, respectively.

Figure captions

Figure 1. Analysis of 3D printing of different ink formulations and pictures of the printed products.

Figure 2. Rheological properties analysis of different ink formulations: (a): viscosity; (b): strain provide information which lines for G′ and G″; (c): storage modulus G′; (d): loss modulus G″.

Figure 3. Microstructure of ink formulations with different magnifications of 1000 ×, 2500 × and 5000 ×.

Figure 4. (a): Changes in molecular interaction force of the composite pastes in the presence of different polysaccharide concentrations. Mean values with different letters (a-d) differ significantly ($p < 0.05$); (b): The Fourier transform infrared, (FTIR) spectrum characterization, (c): X-ray diffractograms and (d): DSC thermograms of composite pastes with different formulations.

Figure 5. The formation mechanism diagram of SPI-polysaccharide composite pastes.

Figure 1

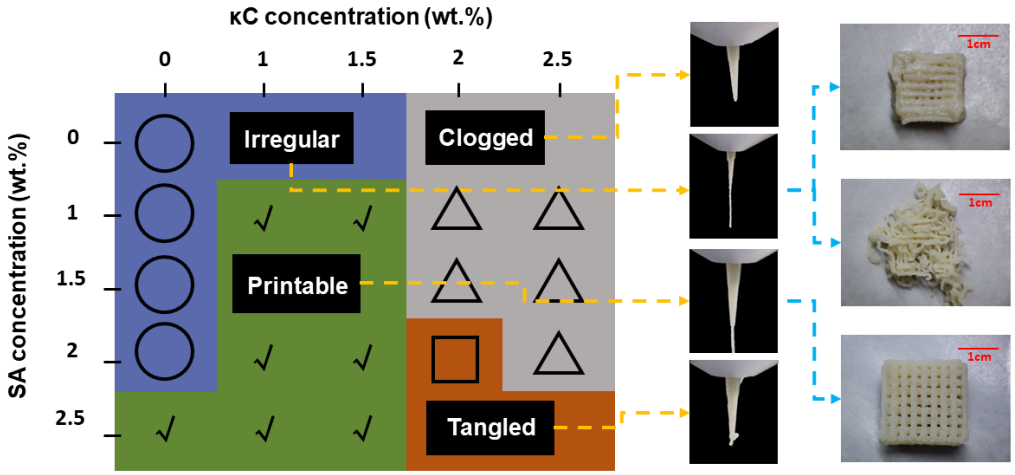

Figure 1. Analysis of 3D printing of different ink formulations and pictures of the printed products.

835 **Figure 2**

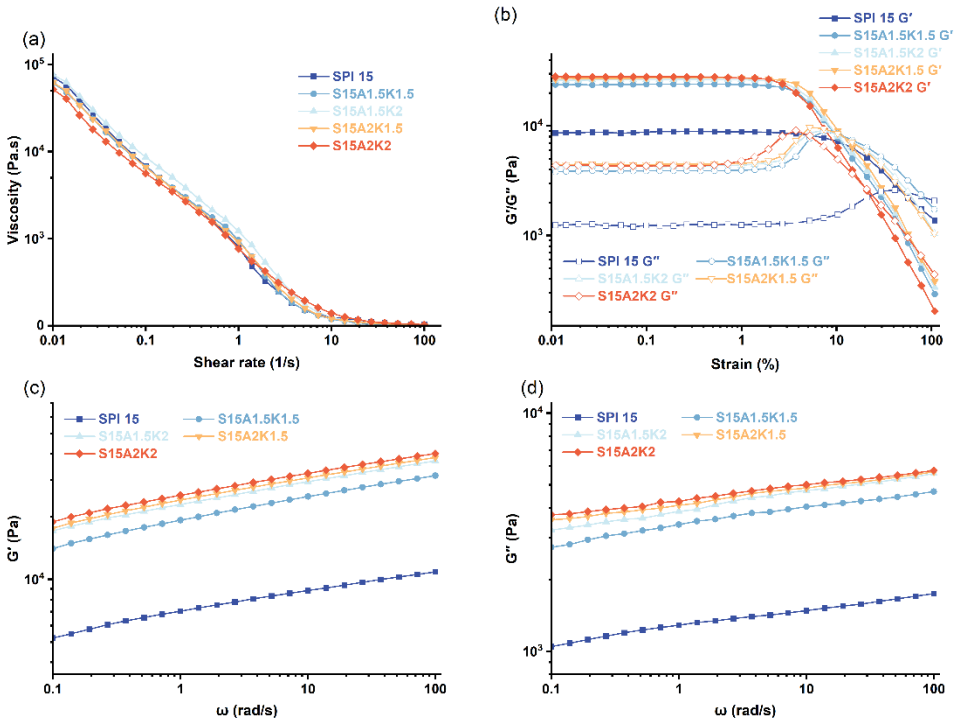

836

837 Figure 2. Rheological properties analysis of different ink formulations: (a): viscosity;

838 (b): strain provide information which lines for G′ and G″; (c): storage modulus G′; (d):

839 loss modulus G″.

840

841 **Figure 3**

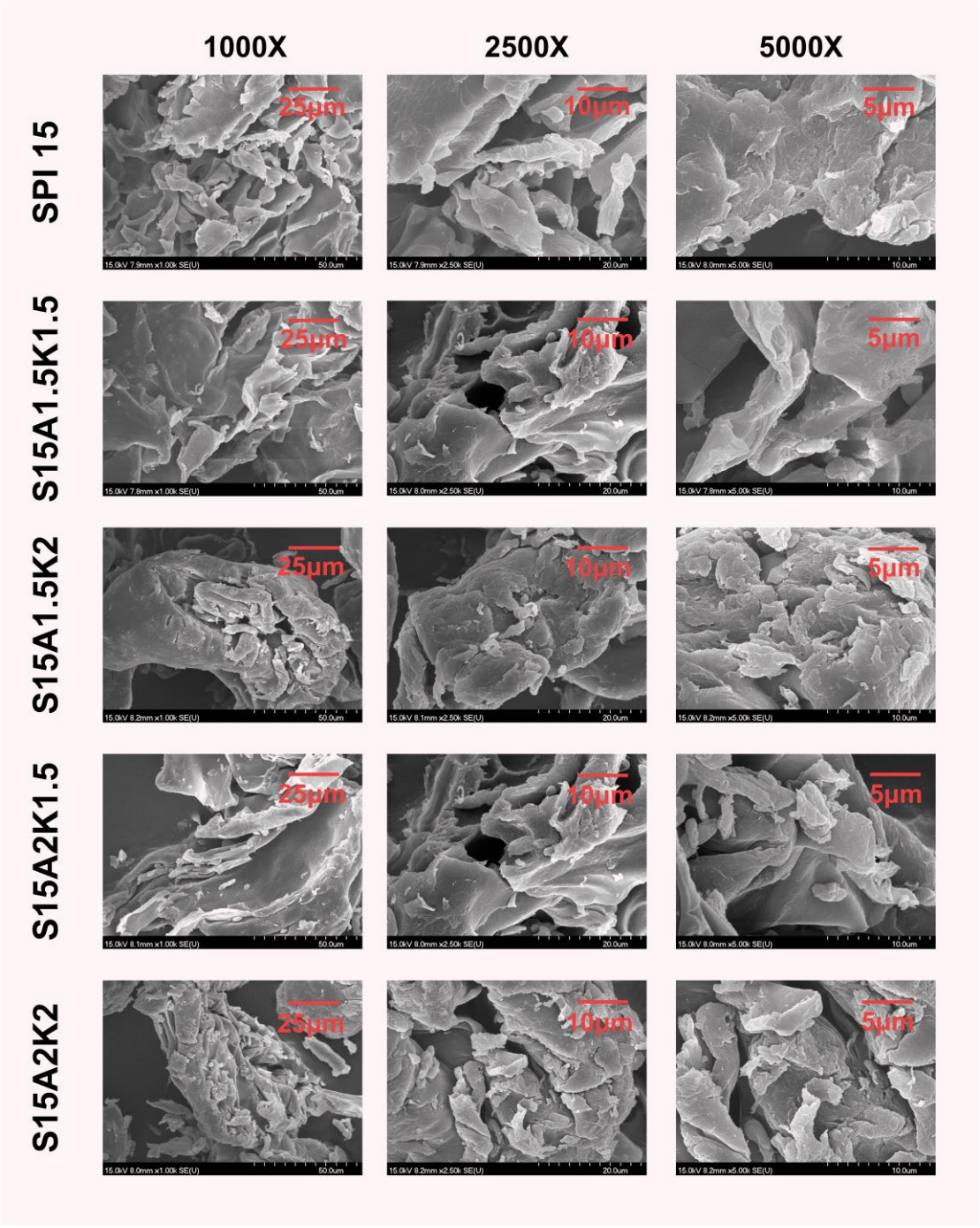

842

843 Figure 3. Microstructure of ink formulations with different magnifications of 1000 ×,

844 2500 × and 5000 ×.

845

Figure 4

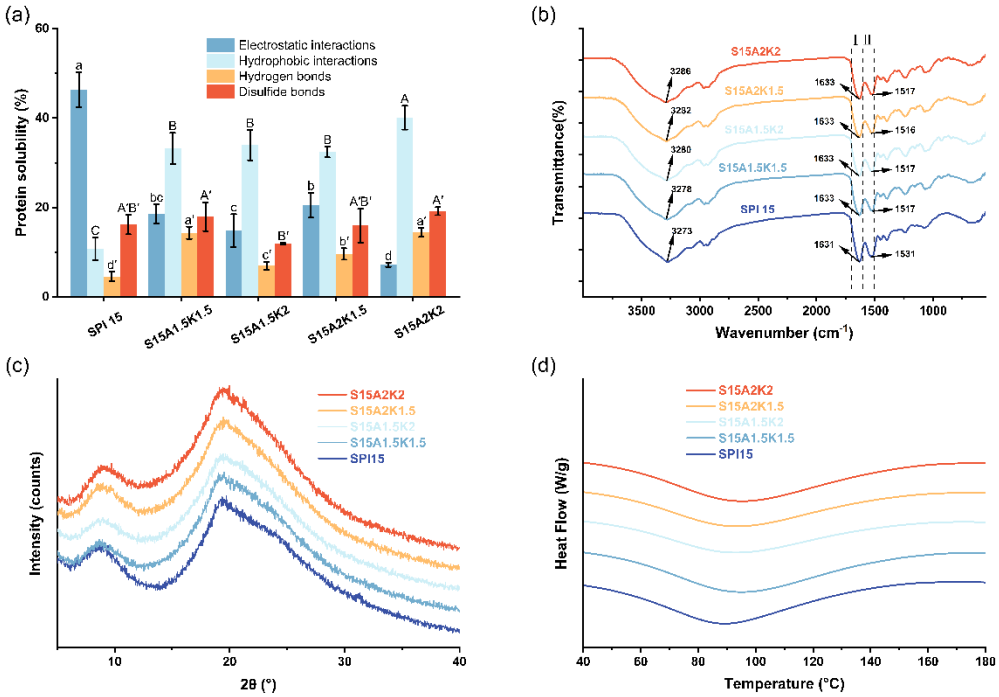

Figure 4. (a): Changes in molecular interaction force of the composite pastes in the presence of different polysaccharide concentrations. Mean values with different letters (a-d) differ significantly ($p < 0.05$); (b): The Fourier transform infrared, (FTIR) spectrum characterization; (c): X-ray diffractograms and (d): DSC thermograms of composite pastes with different formulations.

853 **Figure 5**

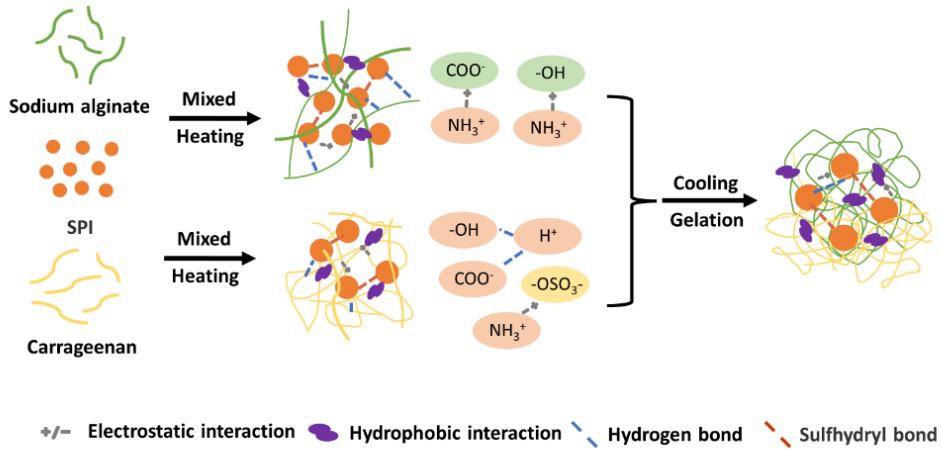

854 Figure 5. The formation mechanism diagram of SPI-polysaccharide composite pastes.